Extrasynaptic signaling enables an asymmetric juvenile motor circuit to produce a symmetric mature gait

Yangning Lu[1,2,a], Tosif Ahamed[2,a], Ben Mulcahy[2], Daniel Witvliet[2,3], Sihui Asuka Guan[1,2], Wesley Hung[2], Jun Meng[1,2], Quan Wen[5,6], Aravinthan DT Samuel[5], and Mei Zhen[1,2,3,4*]

[1]Department of Physiology, University of Toronto, Toronto, ON, Canada, [2]Lunenfeld-Tanenbaum Research Institute, Mount Sinai Hospital, Toronto, ON, Canada, [3]Department of Molecular Genetics, University of Toronto, Toronto, ON, Canada, [5]Department of Physics and Center for Brain Science, Harvard University, Cambridge, MA, USA, [6]School of Life Sciences, University of Science and Technology, Hefei, Anhui, China, [a]These authors contributed equally, [*]Correspondence: meizhen@lunenfeld.ca

Bilaterians generate motor patterns with symmetries that correspond to their body plans. This is thought to arise from wiring symmetries in their motor circuitries. We show that juvenile *C. elegans* larva has an asymmetrically wired motor circuit, but they still generate bending pattern with dorsal-ventral symmetry. In this juvenile circuit, wiring between excitatory and inhibitory motor neurons drives and coordinates contraction of dorsal muscles with relaxation of ventral muscles, producing dorsal bends. Ventral bending is not driven by its own circuitry. Instead, ventral muscles are excited uniformly by premotor interneurons through extrasynaptic signaling, and ventral bends occur in entrainment to the activity of motor neurons for dorsal bends. During maturation, the juvenile motor circuit is replaced by two homologous motor circuits that separately generate dorsal and ventral bending. Our modeling reveals that the juvenile circuit configuration provides an adequate solution for an immature motor circuit to drive functional gait long before the animal matures.

Introduction

Symmetries in an animal's gait patterns are often thought to be driven by wiring symmetries of its motor circuitry mirrored by their body plans. For example, limb movements of vertebrates are driven by multiple rhythmogenic spinal interneuron circuits called the half-centers[1,2]. The left and right half-centers mirror each other structurally. They coordinate contraction and relaxation of muscle groups in the left and right hind-limbs, respectively. Phased relations between the left and right half-centers give rise to gait patterns with left-right alternation[3–6].

C. elegans generates alternating dorsal-ventral bending waves for locomotion. The wiring diagram of its adult motor circuit allows symmetric inputs onto dorsal and ventral body wall muscles. This motor system consists of two homologous motor neuron networks[7,8], analogous to a two half-center configuration. In this circuit, both dorsal and ventral muscles form neuromuscular junctions (NMJs) with the cholinergic excitatory motor neurons (eMNs) that contract muscles, as well as with the GABAergic inhibitory motor neurons (iMNs) that relax muscles[9–11].

One motor subcircuit consists of repeated modules of a subclass of cholinergic eMNs (called DA and DB), and a subclass of GABAergic iMNs (called VD). They are interconnected to coordinate simultaneous dorsal muscle contraction and ventral muscle relaxation in each body segment, producing dorsal bends. A complementary motor subcircuit produces ventral bends, with symmetric wiring of a homologous subclass of cholinergic eMNs (called VA and VB) and GABAergic iMNs (called DD)[8]. Alternating activity of two circuitries in each body segment gives rise to alternating dorsal and ventral bending during adult locomotion.

However, the newly born L1 larva lacks this wiring symmetry (Fig. 1A, B). L1 larva has only DA, DB, and DD motor neurons[12]. A partial serial section electron microscopy (ssEM) reconstruction of the L1 larva[7] suggests that motor neuron wiring is different compared to adults[8]. In the reconstructed body segment, the cholinergic eMNs (DA and DB) make NMJs exclusively to dorsal muscles and the GABAergic iMNs (DD) make NMJs exclusively to ventral muscles. NMJs from the eMN (DA and DB) motor neurons are also dyadic to the iMNs (DD) motor neurons. Hence the L1 motor circuit is wired to resemble the motor circuit for dorsal bends in adult. Despite lacking a homologous circuitry to driven ventral bends, the L1 larva crawls with an adult-like sinusoidal gait. Thus, a L1 larva must have a different solution for generating dorsal-ventral symmetry in its body bending.

Here, we sought mechanisms by which this structurally asymmetric motor circuit gives rise to a symmetric gait. First, we used ssEM to fully reconstruct the connectivity between premotor interneurons, motor neurons, and muscle cells of the L1 motor circuitry along the body. We then used calcium imaging, optogenetics, synapse and cell ablation to assess the role of all cells and signaling pathways in coordinated ventral and dorsal muscle activity and body bends. Last, we combined modeling and behavioral analyses to develop a quantitative understanding of the underlying mechanisms.

We found that the L1's motor neuron network is interconnected both synaptically and extrasynaptically. They form a self-regulated motor subcircuit to generate and exit dorsal bends along the body. Instead of being driven by a mirrored motor subcircuit, ventral bends are produced by entrainment: extrasynaptic transmission from cholinergic premotor interneurons (eINs) excites ventral muscles uniformly along the body of the worm, which allows the same motor circuit to generate complementary ventral bends along the body. We built a model to simulate this alternative circuit mechanism. We found that the model of the L1 circuit represents a temporary solution during animal development that is able to produce an adult-like motor pattern albeit with less flexibility.

We conclude that extrasynaptic transmission and neuron multi-functionality allow a developmentally immature motor circuit to generate a gait which resembles that of a mature animal. These mechanisms are adaptive developmental strategies by which a circuit maintains constant behavioral output despite undergoing substantial structural changes.

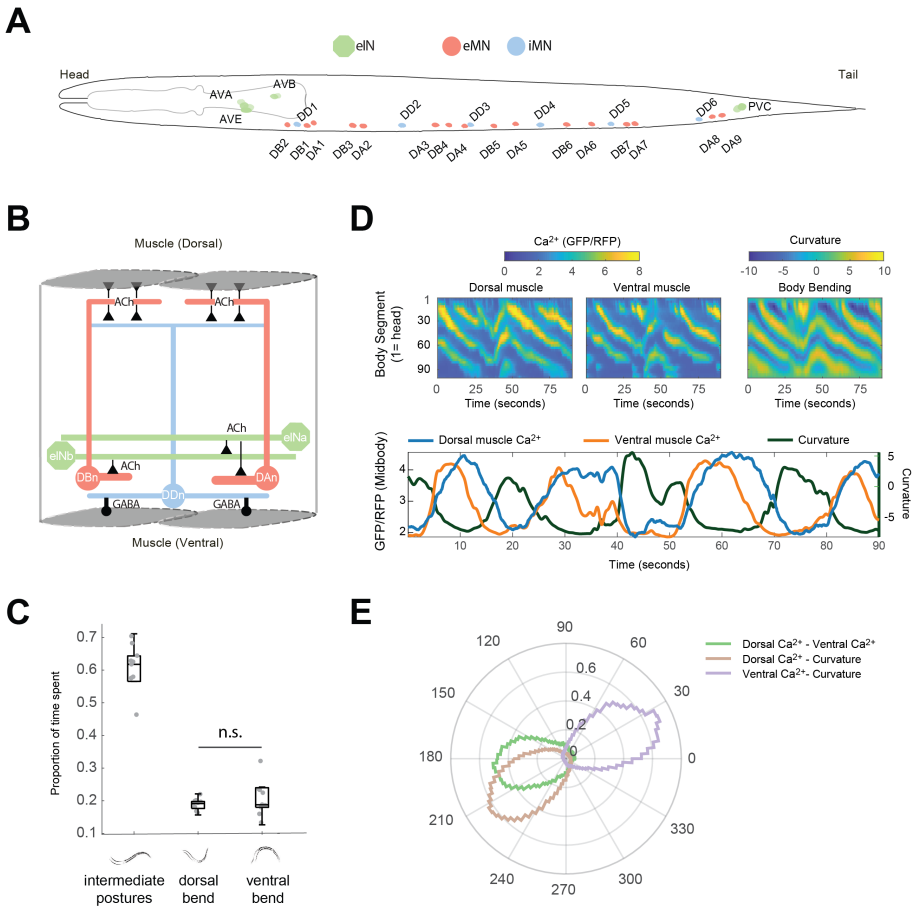

Figure 1. The L1 larva exhibits asymmetry in motor circuit wiring but symmetry in gait pattern and muscle activity. **A.** Schematics of neurons of the motor circuitry for body movement in a newborn *C. elegans* L1 larva. Circles denote neuron soma, color-coded by classes. **B.** Schematics of their synaptic wiring, deduced by serial section transmission EM reconstruction. **C.** Swimming L1 larva alternating dorsal-ventral body bends. **D.** Calcium imaging of a crawling L1 larva's muscle activity in the dorsal and ventral sides. Y-axis represents body segment coordinates. X-axis represents time. Colors represent the GCaMP3/RFP ratio in muscles (top left panels) and the body curvature (top right panel), respectively. Time series of curvature, dorsal and ventral muscle activity at mid-body (segment 50) were plotted in the lower panel. **E.** Polar histograms of the phase difference between curvature, dorsal muscle activity, and ventral muscle activity in the body (segments 33-95). n = 12 larvae.

Results

The L1 motor circuit has asymmetric wiring to dorsal and ventral body wall muscles

C. elegans is born with only a fraction of motor neurons of the adult motor circuit. Beginning at the mid-L1 larva stage, post-embryonic neurogenesis gives rise to new motor neurons[13]. Because the post-embryonic neurons include all that innervate ventral body wall muscles in the adults[8], the L1 larva must have a distinct, and potentially asymmetrically wired motor circuit.

We used ssEM to fully reconstruct the motor circuit of multiple L1 larvae, from premotor interneurons to motor neurons and to muscles (Fig. 1; Fig. S1; Mulcahy *et al*., in preparation). For motor neurons, we confirmed the conclusion from a previous partial reconstruction[7]: inputs to dorsal and ventral muscles are fundamentally asymmetric (Fig. 1B). All cholinergic eMNs (DAs and DBs) make NMJs only to dorsal muscles. All GABAergic iMNs (DDs) make NMJs only to ventral muscles. Most NMJs from the eMN motor neurons (DAs and DBs) are dyadic, innervating dorsal muscle cells as well as the iMN motor neurons (DDs) that project to the opposite side of the body (examples in Fig. S1). Multiple eMNs and iMNs form a chain of similarly wired modules along the body (illustrated in Fig. 1A, B).

In the adult motor circuit, two different groups of premotor interneurons (eINs) innervate the A- and B-class eMNs to regulate directional locomotion[14,15]. Our EM reconstruction revealed that this wiring pattern is already present in the newborn L1 larva (Fig. 1B; Fig S1). The DA subclass of eMN motor neurons are postsynaptic to cholinergic eINs that regulate backward locomotion (AVA, AVE, AVD); the DB subclass eMN motor neurons are postsynaptic to eINs that promote forward locomotion (AVB and PVC). Thus the key difference between the L1 and adult motor circuit's structural wiring resides at the layer between motor neurons to muscles.

L1 larvae generate alternating dorsal-ventral body bends and muscle activities

Despite a dorsal-ventral wiring asymmetry, *C. elegans*'s alternating dorsal-ventral bending pattern is established at birth. When swimming, L1 larvae exhibited sinusoidal bending waves without overt bias for full-body dorsal or ventral coils (Fig. 1C; Supplemental movie 1). When crawling, L1 larvae propagated alternating dorsal-ventral bending waves along the body (Fig. 1D; E; Supplemental movie 1).

Calcium dynamics of body wall muscles correlates with this alternating bending pattern. We examined the calcium

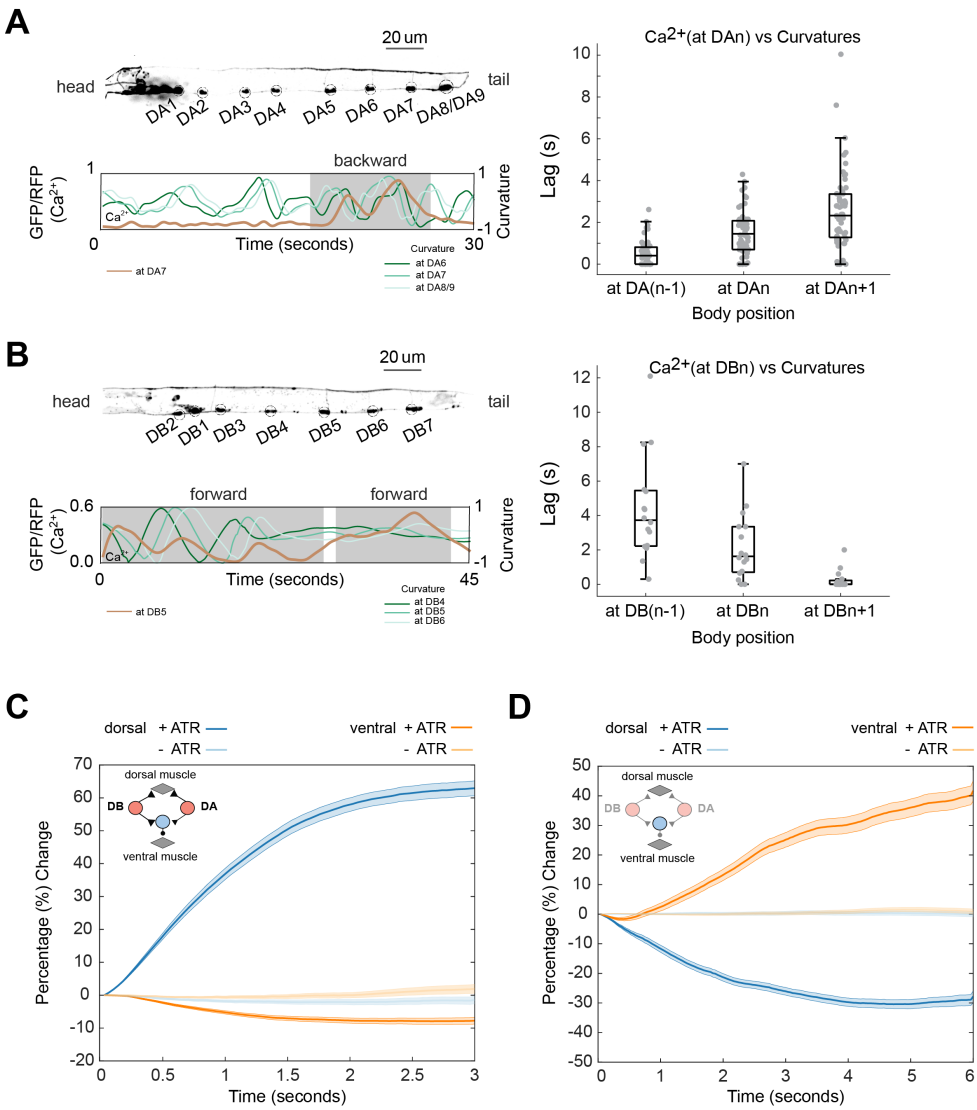

Figure 2. Cholinergic eMN motor neurons underlie dorsal muscle contraction. **A.** Left panel: (Upper) The expression pattern of a GCaMP6s calcium reporter for the DA subclass eMN motor neurons in a newborn L1. (Lower) An example trace of calcium activity for DA7 motor neuron, overlaid with curvatures at different body segments over time. Shaded areas denote periods of backward movement. Y-axis denotes the GCaMP6/RFP ratio at DA7 soma on the left side, and curvature at segments anterior, at, and posterior to DA7 soma on the right side. Right panel: Minimal time lags between calcium activity and curvature changes at regions anterior (N-1), at (N), and posterior (N+1) to the soma of a DA (DAn). **B.** Left panel: (Upper): Expression pattern of a GCaMP6s calcium reporter for the DB subclass eMN motor neurons. This reporter is also expressed in the DA motor neurons but at a lower level than DB in L1 larva. (Lower): an example calcium trace for DB5 motor neuron, overlaid with curvatures at different body segments over time. Right panel: Minimal time lags between calcium activity and curvature changes at body segments anterior (N-1), at (N), and posterior (N+1) to the soma of a DB (DBn). **C.** Simultaneous activation of eMN motor neuron (DA and DB) by Chrimson[16] and calcium imaging of body wall muscles in L1 larvae. Y-axis, muscle activity changes, represented by percentage changes of the GCaMP6/RFP ratio normalized against its value at t=0. X-axis, time in seconds. Control group (-ATR): n = 21 stimulation from 7 larvae. Experimental group: (+ATR): n = 33 stimulation from 12 larvae. **D.** Simultaneous inactivation of eMN motor neurons by GtACR2[17] and calcium imaging of body wall muscles in L1 larvae. Control group (-ATR): n = 39 stimulation from 8 larvae. Experimental group (+ATR): n = 35 stimulation from 12 larvae. Lines and shades denote medium and 95% confidence intervals, respectively.

dynamics of body wall muscles in slowly crawling L1 larvae (Fig. S2; Supplemental movie 2). When they crawled, calcium waves propagated along the dorsal and ventral body wall muscles (Fig. 1D). In each body segment, calcium activity changes in dorsal and ventral muscles correlated with curvature changes during dorsal and ventral bending, respectively (Fig. 1E). Specifically, the dorsal-ventral alternation in body bending correlated with an out-of-phase activation pattern of the dorsal and ventral body wall muscles (Fig. 1E). Maximum cross-correlation between dorsal muscle activity and bending, and between ventral muscle activity and bending exhibit significant phase shifts (Fig. 1D, E). The extent of this phase shift depended on the larva's crawling speed (Fig. S2).

Cholinergic excitatory motor neurons drive dorsal muscle contraction

Wiring asymmetry of the L1 motor circuit needs to be reconciled with the bending symmetry of the L1 larva. One hypothesis is that the functional relationship between L1 motor neurons and muscle cells are altered in a way that compensates for the wiring asymmetry. To determine the functional relationship between cholinergic motor neurons and bending, we first examined correlations between calcium dynamics of eMN motor neurons, DA and DB, with dynamics of bending.

We found that when L1 larvae moved backwards, DA motor neurons were activated in an anterograde sequence as bending traveled from tail to head (Fig. 2A; Supplemental movie 3). Calcium dynamics at each DA soma correlated with dorsal

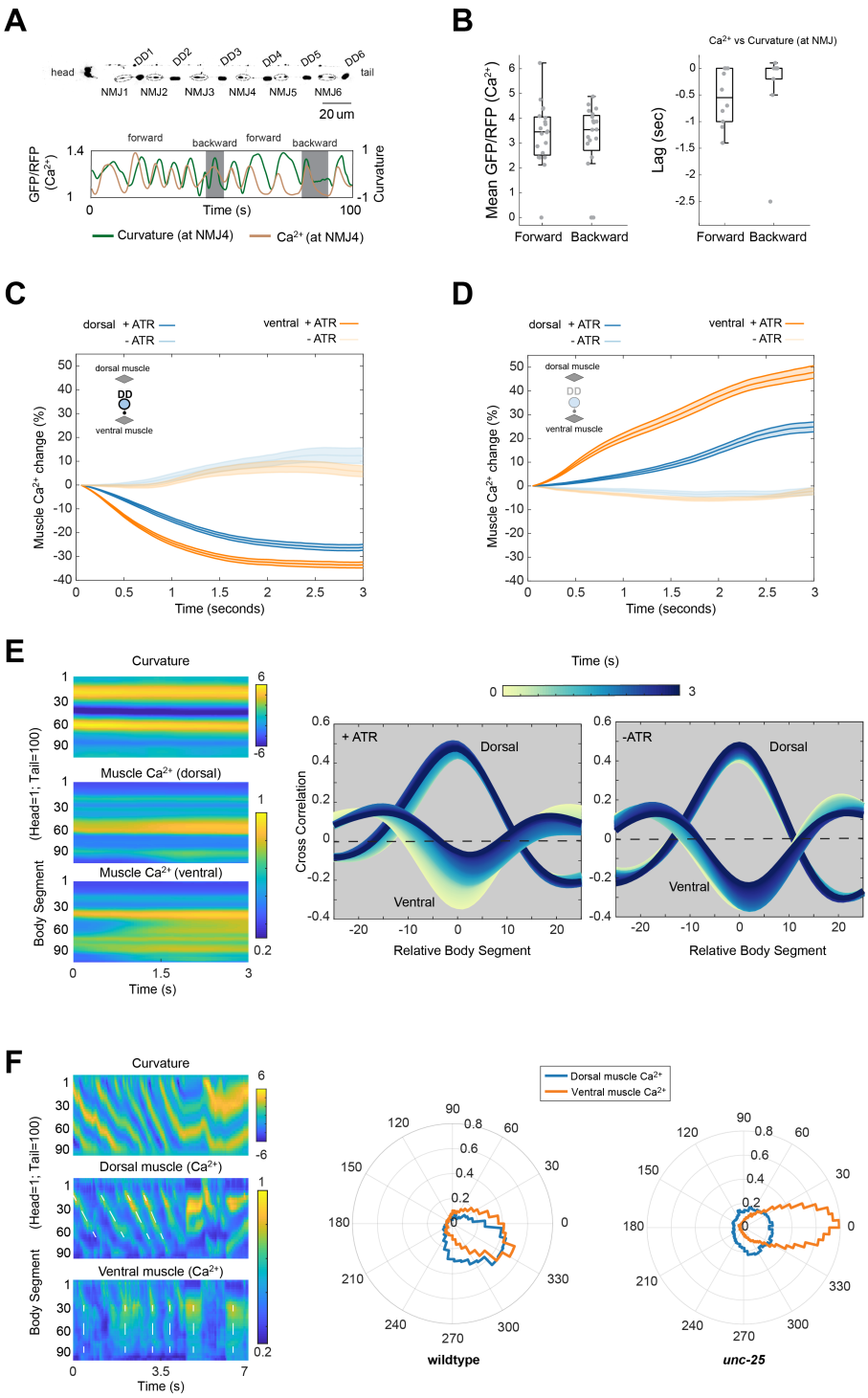

Figure 3. GABAergic iMN motor neurons underlie ventral and dorsal muscle relaxation A. (Upper) A GCaMP reporter for DD motor neurons. Each DD makes a tight cluster of NMJs; synapses and soma from the same DD neuron are marked as NMJ and DD, follow by the same number. (Lower) An example calcium trace of NMJ4, synapse from DD4, overlaid with body curvature anterior, at, and posterior to where NMJ4 resides. Periods of backward movements are marked by grey bars. **B.** (Left) Mean calcium activity of DD NMJs, represented by averaged GCaMP6/RFP ration during periods of forward and backward movements. n = 17 NMJ clusters from 12 larvae; (Right) Minimal time lags between calcium activity and curvature changes during forward and backward movements. **C.** Simultaneous GABAergic iMN (DD NMJs) Chrimson activation and muscle calcium imaging in L1 larvae. Y-axis represent percentage change of activity at a NMJ cluster, represented by GCaMP/RFP ratio, normalized against the value at the first frame (t0). X-axis represents time. Control group (-ATR): n = 13 stimulation from 7 larvae; Experimental group (+ATR): n = 18 stimulation from 10 larvae. **D.** Simultaneous GABAergic iMN (DD) GtACR2 inhibition and muscle calcium imaging in L1 larvae. Control group (-ATR): n = 10 stimulation from 5 larvae; Experimental group (+ATR): n = 19 stimulation from 10 larvae. Lines and shades in C and D represent medium and 95% confidence interval. **E.**(Left) An example heatmap representation of the dorsal and ventral muscle activity and curvature of an animal during iMN GtACR2 inactivation. (Right) Cross correlation between the muscle calcium signal along the body with curvature at one point in time. Color encodes time during the course of iMN inactivation. The peak cross-correlation tends towards zero for ventral muscle calcium. **F.** (Left) An example recording of dorsal and ventral muscle activities in a crawling mutant larva that cannot synthesize GABA (*unc-25*). Dashed lines denote none-propagating ventral muscle activity. (Right) Polar histograms of phase differences of muscle activity along the dorsal and ventral body of wildtype and *unc-25* L1 larva.

bending, exhibiting the shortest time lag with that of the anterior body segment (Fig. 2A, right panel). This position-dependent correlation is consistent with the anatomical wiring: axons of DA motor neurons project

anteriorly, making NMJs to dorsal muscles anterior to its soma (Fig. 1B).

When L1 larvae moved forward, DB motor neurons were activated in a retrograde sequence as bending travelled from head to tail (Fig. 2B; Supplemental movie 4). Calcium dynamics at each DB soma correlated with dorsal bending, exhibiting the shortest time lag with that of the posterior body segment (Fig. 2B, right panel), consistent with the posterior projection of the DB axons (Fig. 1B). Both results establish positive correlations between the activity of cholinergic eMN motor neurons and dorsal bending.

To determine whether eMN motor neurons directly activate dorsal muscles, we imaged calcium dynamics in body wall muscles while simultaneously manipulating motor neuron activity (see Methods). We found that co-activation of all eMN motor neurons by Chrimson increased the activity of dorsal muscles, but not ventral muscles (Fig. 2C). Similarly, inhibition of eMN motor neurons by GtACR2 lowered the activity of dorsal muscles, but not ventral muscles (Fig. 2D). Cholinergic inputs from eMN motor neurons are thus excitatory specifically to dorsal muscles.

GABAergic iMN motor neurons promote ventral and dorsal muscle relaxation

GABAergic iMN motor neurons (DD) make NMJs exclusively to ventral body wall muscles. During early postnatal development, GABAergic synapses from rodent interneurons not inhibitory but excitatory[18]. In the L1 larva, whether GABAergic signaling inhibits muscle contraction, as in the adult, remains inconclusive[19,20].

To assess how DD motor neurons regulate muscle activity, we examined correlation between their calcium dynamics and ventral bending in crawling L1 larvae. Through EM analyses, we found that each DD motor neuron makes a tightly spaced cluster of NMJs. We could record calcium dynamics in each cluster as a single area of interest (ROI) (Fig. 3A, NMJn). These NMJs were equally activated when animals moved forward and backward (Fig. 3B; Supplemental movie 5). During both directional movements, their activation correlated with ventral relaxation. Specifically, a calcium rise preceded an decreased curvature at each ROI (Fig. 3B).

To directly examine their effect on ventral muscle activity, we measured muscle calcium dynamics upon optogenetic manipulation of DD motor neurons. As expected from inhibitory NMJs, activation of DD motor neurons by Chrimson strongly reduced ventral muscle activity (Fig. 3C). Unexpectedly, DD activation also led to a smaller reduction of dorsal muscle activity (Fig. 5B), even though they do not make NMJs to dorsal muscles (Fig. 3B). Inhibition of DD motor neurons by GtACR2 had an analogous effect in reverse: a strong increase in ventral muscle activity, accompanied by a smaller increase in dorsal muscle activity (Fig. 3D; Supplemental movie 6). More intriguingly, during the inhibition, activity increase of ventral and dorsal muscles exhibited spatial difference (Supplemental movie 6). Ventral muscle activity increase took place uniformly across the body, decreasing correlations with curvature over time, whereas dorsal muscle activity continued to increase in accordance with curvature (Fig. 3E).

The difference effects of DD manipulation on ventral and dorsal muscle activity is not an artifact of optogenetic manipulation of DD motor neurons. In mutant larvae that do not synthesize GABA (*GAD/unc-25*), we observed similar differences between dorsal and ventral muscles (Supplemental movie 7). In a crawling *unc-25* L1 larva, dorsal muscles exhibited calcium dynamics that correlated with propagating bending waves, whereas calcium signals of ventral muscles did not propagate, disrupting such correlation with curvature(Fig. 3F; Fig. S3).

These results establish that GABAergic DD motor neurons are inhibitory at birth. These iMN motor neurons inhibit ventral muscles with NMJs and dorsal muscles without direct synaptic input. Dorsal and ventral muscles exhibit structural, temporal and spatial differences in their relationships with iMN motor neurons. These differences implicate distinct inhibitory mechanisms.

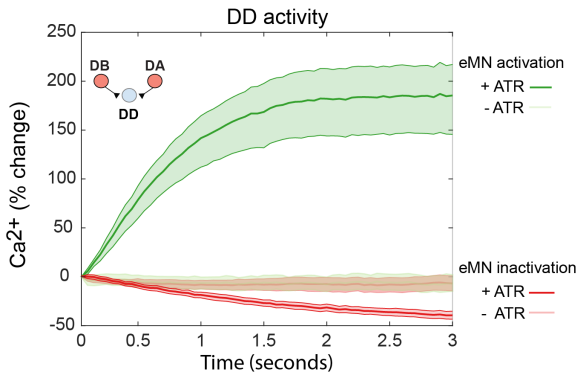

Figure 4. Wiring between cholinergic and GABAergic motor neurons coordinates dorsal bending Schematics depicting simultaneous optogenetic manipulation of eMN (DA and DB cholinergic motor neurons) and calcium imaging of iMN (DD NMJs). Upper traces: activation of eMNs by Chrimson elevates iMN activity. -ATR group: n = 20 stimulation from 5 larvae; +ATR group: n = 23 stimulation from 9 larvae. Lower traces: inhibition of eMNs by Archaerhodopsin decreases DD activity. -ATR group: n = 25 stimulation from 6 larvae; +ATR group: n = 21 stimulation events from 9 larvae.

eMN and iMN motor neurons form a motor circuitry for dorsal bending

Most NMJs from the eMN motor neurons to dorsal muscles are dyadic synapses, juxtaposing the dendrite of iMN motor neurons that inhibits the opposing ventral muscles (Fig. S1). Thus, activation of dorsal muscles should lead to simultaneous inhibition of contralateral ventral muscles.

Consistent with this hypothesis, activation of all eMN motor neurons by Chrimson increased iMN motor neuron's activity (Fig. 4; Supplemental movie 8a). Inhibition of all eMN motor neurons by GtACR2 decreased iMN motor neuron's activity (Fig. 4; Supplemental movie 8b). Furthermore, anatomic ablation of the DB subclass eMN motor neurons by miniSOG[21] preferentially reduced DD motor neuron's activity when animals attempted to move forward, whereas ablation of the DA subclass eMN motor neurons reduced DD motor neuron's activity when animals attempted to move backward (Fig. S4).

We have shown that NMJs to dorsal and ventral muscles drive their contraction and relaxation, respectively (Fig. 2 and Fig. 3). Dyadic NMJs from eMN motor neurons to iMN motor neurons would thus promote the relaxation of juxtaposed ventral muscles when dorsal muscles contract. This coordination promotes dorsal bending (Fig. 4). Cholinergic

eMN motor neurons are oscillators in the adult motor circuit[22–24]. Thus, synaptic wiring of the L1 motor neurons forms one half-center that makes the body bend dorsally.

Extrasynaptic inhibition from iMN motor neurons promotes exit from dorsal bending

We have shown that GABAergic iMN motor neurons inhibit both ventral and dorsal muscles, with different kinetics (Fig. 3). iMN motor neurons make inhibitory NMJs to ventral muscles, but they do not make synapses to dorsal muscles, or to cholinergic motor neurons that activate dorsal muscles (Fig. 1B; Fig. S1). This raises the possibility of extrasynaptic signaling.

Synaptic and extrasynaptic GABA inhibition involves ionotropic $GABA_A$ and metabotropic $GABA_B$ receptors, respectively[25–27]. Consistent with previous reports[28,29], in the newborn L1 larva, the $GABA_A$ receptor (UNC-49) is present in ventral muscles and not in dorsal muscles (Fig. 5D). Along the ventral body, endogenously tagged UNC-49 formed six clusters (Fig. 5D), reminiscent of the clustered NMJs by individual DD motor neurons (Fig. 3A. In $GABA_A$-(*unc-49*) mutant larvae, inhibition of ventral muscles induced by iMN motor neuron activation was significantly attenuated, but the inhibition on dorsal muscles was only modestly reduced (Fig. 5A, B). Thus the $GABA_A$ receptor is critical for inhibitory NMJs to ventral muscles and less so for dorsal muscles.

In the $GABA_B$-(*gbb-2*) mutant larvae, inhibition of dorsal muscles upon iMN motor neuron activation was potently attenuated, whereas inhibition of ventral muscles unaffected (Fig. 5A, B). Thus, $GABA_B$ receptors play a predominant role in dorsal muscle relaxation. We found that the $GABA_B$ receptor, a GBB-1/GBB-2 complex, is more broadly expressed than the $GABA_A$/UNC-49 receptors in the L1 larva. GBB-2::GFP is present in many neurons including cholinergic eMN motor neurons, as well as in body wall muscles (Fig. 5D).

Inhibition of dorsal muscles was not fully abolished in either *unc-49* or *gbb-2* mutant larva. Only in L1 larva that lacks both $GABA_A$ and $GABA_B$ receptors, iMN motor neuron activation fully failed to inhibit dorsal and ventral muscles (Fig. 5A, B). Mutant L1 larvae that do not synthesize GABA recapitulated this response (Fig. S5).

Despite making a minor contribution to dorsal muscle inactivation, $GABA_A$ receptors controlled the rate of inhibition in both ventral and dorsal muscles (Fig. 5C). Together, these results demonstrate that iMN motor neurons indirectly relax dorsal muscles. Extrasynaptic inhibition to eMN motor neurons works in concert with synaptic inhibition to ventral muscles to promote an exit after dorsal bending.

Specifically, when eMN motor neurons activate dorsal muscles, iMN motor neurons are co-activated to relax contralateral ventral muscles through inhibitory NMJs. iMN motor neurons also signal extrasynaptically, simultaneously reducing eMN motor neuron's activity through $GABA_B$ receptors. This negative feedback promotes dorsal muscle relaxation following ventral muscle relaxation.

Therefore, in the L1 larva, motor neurons form a circuit where synaptic wiring drives dorsal bending. This circuit regulates its own exit from dorsal bending through a negative feedback in part by extrasynaptic GABA signaling.

Ventral muscle excitation requires cholinergic eIN premotor interneurons

A motor circuit to drive dorsal bending and its own exit does not produce ventral bending. Ventral bending requires ventral muscle contraction that occurs in synchrony with dorsal muscle relaxation. Other mechanisms must excite ventral muscles in order for the L1 motor circuit to transit from dorsal to ventral bending.

To reveal this mechanism, we first considered the simplest possibility: a higher myogenic activity of ventral muscles compensates for the absence of motor neuron excitation. However, we found that optogenetic inhibition of L1 larva's entire nervous system led to similarly silenced dorsal and ventral muscles (Fig. S6A). This shows that ventral muscle activity is not myogenic, but is driven by neurons.

To identify neurons that excite ventral muscles, we turned to optogenetic stimulation. Because ventral muscles receive inhibitory NMJs from GABAergic iMN motor neurons, in the wildtype larva, pan-neuronal excitation activated dorsal muscles but inhibited ventral muscles (Fig. S6C, left panel). In the L1 larva that does not synthesize GABA (*GAD/unc-25*), however, we observed activation of both ventral and dorsal muscles (Fig. S6C, right panel). This assay can be applied to identify the neuron source for ventral muscle activation.

We next examined whether the excitatory input to ventral muscles is cholinergic. We found that optogenetic manipulation of all cholinergic neurons recapitulated the effects of pan-neuronal manipulation: pan-cholinergic inhibition by GtACR2 abolished activity equally in dorsal and ventral muscles (Fig. S6B). Pan-cholinergic stimulation by Chrimson activated both dorsal and ventral muscles in the mutant larva without GABA (*unc-25*) (Fig. S6D, right panel), but led to dorsal muscle excitation and ventral muscle inhibition in wildtype larvae (Fig. S6D, left panel). Thus, cholinergic neurons are responsible for ventral muscle activation.

We have shown that cholinergic eMN motor neurons do not innervate ventral muscles (Fig. 2). Axons of several premotor interneurons (eINs) are cholinergic[30], and span the entire ventral nerve cord, making them the candidate source of ventral muscle excitation. Among eIN premotor interneurons, two (AVA and PVC) make numerous synapses to all cholinergic eMN motor neurons along the ventral nerve cord. Others (AVB, AVE, AVD) make synapses onto them and to one another along the ventral nerve cord (Fig. 1B).

We found that optogenetic inhibition of eIN premotor interneurons by GtACR2 silenced both dorsal and ventral muscles (Fig. 6B; Supplemental movie 9). In mutant larvae without GABA, optogenetic stimulation of eINs activated both dorsal and ventral muscles, with ventral muscles exhibiting a higher percentage of increase (Fig. 6A; Supplemental movie 10). Patterns of dorsal and ventral muscle activity also differed: dorsal muscle activity rise was in correlation with local curvature whereas ventral muscle activity rise was uniform along the body (Supplemental movie 10). Similar distinction was observed during optogenetic silencing of iMN motor neurons in wildtype L1 larvae (Fig. 3D). These results suggest that ventral muscles may be uniformly activated long the body by extrasynaptic cholinergic signaling from the eIN premotor interneurons.

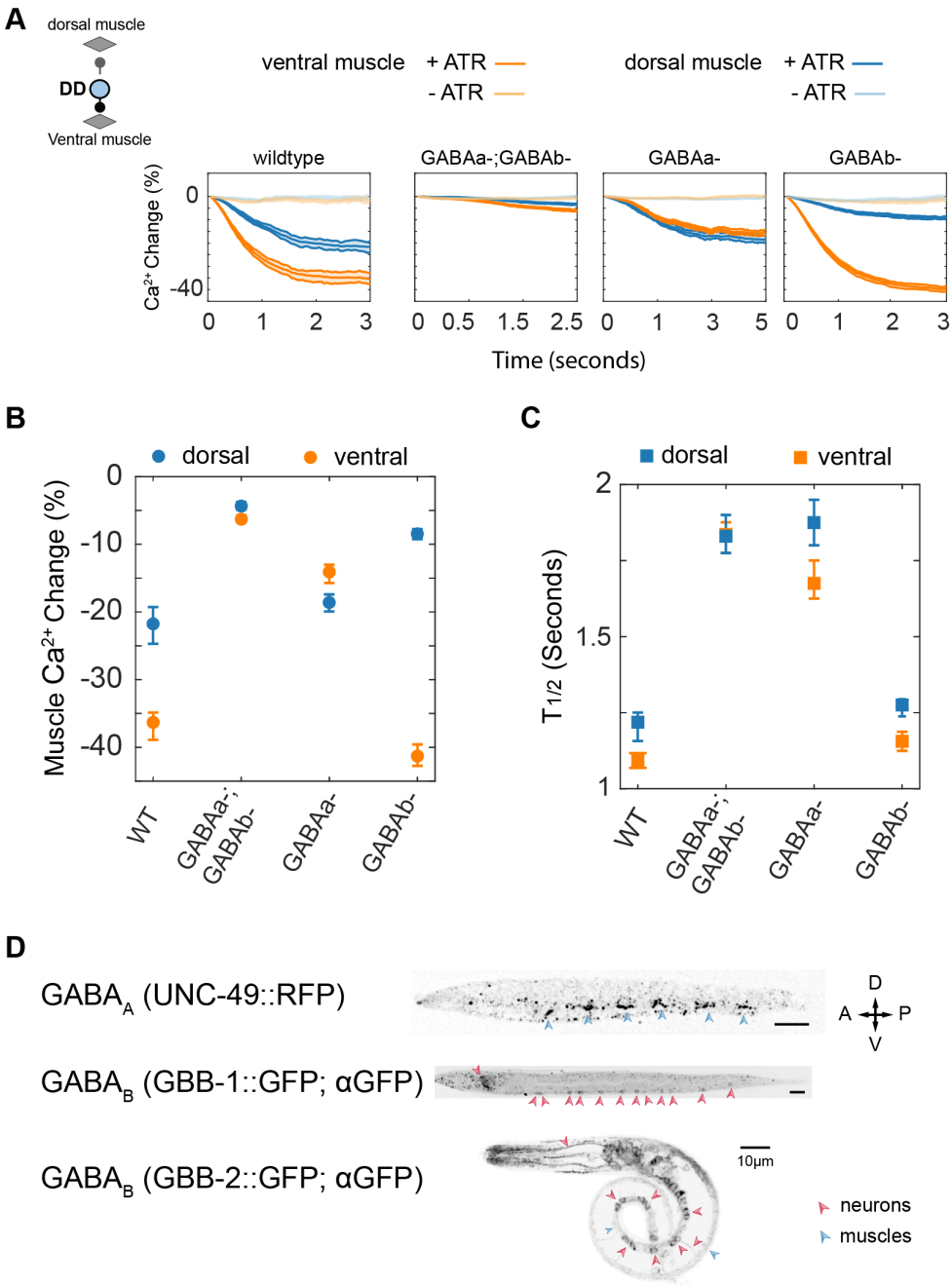

Figure 5. Ionotropic and metabotropic GABA signaling inhibit ventral and dorsal muscles, respectively A. Top: Schematics depicting simultaneous optogenetic activation of iMN motor neurons (DD) and muscle calcium imaging. Bottom: DD motor neuron activation in wildtype L1 larvae reduces both dorsal and ventral muscle activities; these reductions were differentially attenuated in mutant larvae that lack ionotropic GABAa receptors (*unc-49(e407)*(Control group (-ATR): n = 37 stimulation events from 22 larvae; Experimental group (+ATR): n = 51 stimulation events from 20 larvae), metabotropic GABAb receptors (*gbb-2(tm1165)*) (Control group (-ATR): n = 18 stimulation events from 6 larvae; Experimental group (+ATR): n = 39 stimulation events from 7 larvae), or both (*unc-49(e407);gbb-2(tm1165)* (Control group (-ATR): n = 46 stimulation from 12 larvae; Experimental group (+ATR): n = 76 stimulation from 19 larvae). Lines and shades denote medium and 95% confidence intervals. **B** Maximal activity changes in dorsal and ventral muscles in respective genotypes shown in A. **C** Half-time constants of the dorsal and ventral muscle activity changes in respective genotypes shown in A. **D** Expression patterns of endogenously tagged GABAa::RFP receptors and GFP tagged fosmid reporters for two subunits of a heterologous GABAb receptor complex, GBB-1::GFP and GBB-2::GFP.

To further determine whether eIN premotor interneurons are required for ventral muscle activation, we ablated them using miniSOG. All eIN-ablated L1 larvae exhibited diminished ventral muscle activities, but with residual dorsal muscle activities (Fig. 7A; Supplemental movie 11). When inhibitory input to ventral muscles was removed in *unc-25* mutant larvae, ablation of eIN premotor interneurons also diminished ventral muscle activity, while leaving dorsal activity intact (Fig. 7B; Supplemental movie 13). Reducing ventral muscle activity confirms that eIN premotor interneurons are required for ventral muscle excitation. Persistent dorsal muscle activity is consistent with the presence of endogenous eMN motor neuron activities, as previously observed in the adult motor circuit[22,23]. These results establish the requirement of eIN premotor interneurons in stimulating ventral muscles.

Cholinergic eIN premotor interneurons activate ventral muscles via extrasynaptic signaling

Because eIN premotor interneurons do not make synapses to ventral muscles (Fig. 1B; Fig. S1), they may activate ventral muscles by ephaptic coupling or by extrasynaptic mechanisms that require neurotransmitter release.

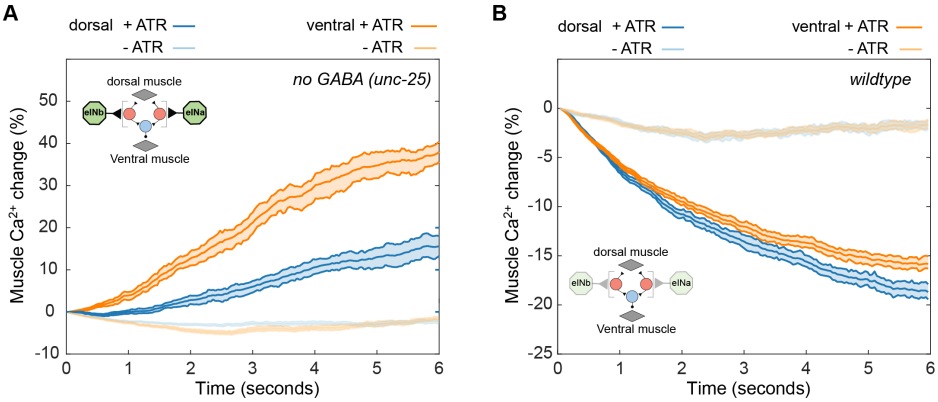

Figure 6. Cholinergic eIN premotor interneurons underlie ventral muscle contraction A Simultaneous muscle calcium imaging upon eIN optogenetic activation in *unc-25* L1 larvae. Activation of eINs by Chrimson elevates both dorsal and ventral muscle activity. Control group(-ATR), n = 51 stimulation from 17 larvae; Experimental group(+ATR): n = 43 stimulation from 12 larvae. **B** Simultaneous muscle calcium imaging upon optogenetic eIN inhibition in wildtype L1 larvae. Inhibition of eINs by GtACR2 reduces both dorsal and ventral muscle activity. Control group(-ATR): n = 28 stimulation from 6 larvae; Experimental group(+ATR): n = 49 stimulation from 13 larvae.

We distinguished these two possibilities by assessing the effect of blocking synaptic vesicle fusion by tetanus toxin (TeTx)[31]. When vesicular release from all eIN premotor interneurons was blocked, activity in both dorsal muscles and ventral muscles was reduced (Fig. 7C; Supplemental movie 14). Vesicular release is needed for eIN premotor interneurons to activate dorsal muscles because they innervate cholinergic eMN motor neurons, as expected. Reduced ventral muscle activation, however, demonstrates that vesicular neurotransmitter release is also needed for eIN premotor interneurons to activate ventral muscles. Similar to effects of eIN ablation, ventral muscle activity was more severely reduced than dorsal muscles (Fig. 7C, middle panel). These results argue for the requirement of extrasynaptic accumulation of acetylcholine to drive ventral muscle activation. An extrasynaptic accumulation of acetylcholine is also consistent with the observed uniform increase of ventral muscle activity during eIN premotor interneuron stimulation.

Together, these results establish that cholinergic eIN premotor interneurons stimulate ventral muscles, likely through extrasynaptic acetylcholine accumulation.

One motor subcircuit orchestrates dorsal-ventral bend symmetry

Our data demonstrated that synaptic wiring among motor neurons is built to make only dorsal bends, but with ventral muscles tonically activated, the same circuitry can simultaneously entrain ventral muscles to generate complementary ventral bends. An implication of this model is that ventral muscle excitation takes places independently of motor neurons, but the larva requires synaptic wiring among motor neurons to generate coordinated dorsal-ventral bending.

Consistent with this implication, we found that blocking synaptic transmission from eMN motor neurons and eIN premotor interneurons by TeTx led to opposite effect on muscle activity. Eliminating eINs or their synaptic output resulted in dorsal muscle activity to be higher than ventral muscle activity (Fig. 7C), whereas eliminating eMN output led to ventral muscle activity to be higher than dorsal muscle activity (Fig. 7D).

Behaviorally, however, only dorsal muscle's calcium signals, reflecting direct input from eMN motor neurons, predicts a crawling larva's bending pattern.

When eIN premotor neurons or their synaptic output were eliminated, regardless of the absolute level of residual dorsal activity, they led to persistent bias for dorsal bending across body segments, in both wildtype and *unc-25* mutant larvae (Fig. 7A-C; Supplemental movie 11-13).

When eMN synaptic output was perturbed, regardless of the higher ventral muscle activity (Fig. 7D), L1 larvae exhibited no consistent dorsal or ventral bias across body segments (Fig. 7D; Supplemental movie 14). This coincides with a spatially uniform calcium signals in their ventral muscles that lacked correlation with curvatures (Fig. 7D). Absence of correlation is similar to the calcium pattern of ventral muscles in the *unc-25* mutant larvae (Fig. 3D).

Interestingly, when eMN synaptic output was perturbed, average calcium activity in ventral muscles was significantly higher than in wildtype larva (Fig. 7D). Average dorsal muscle activity was reduced, but only modestly compared to the level in the wildtype larva (Fig. 7D). These anomalies could not be explained by a partial blockage of eMN synaptic transmission because these larvae were severely compromised in mobility (Supplemental movie 14). We speculate that calcium signals in eMN-TeTx animals reflect an endogenous embryonic myogenic activity[32,33] that lingers due to the absence of synaptic input from motor neurons.

Simulation of an alternative model for symmetric motor patterns

A functional model of how bending is generated within each segment is illustrated below (Fig. 8A). Anatomic wiring of the L1 motor circuit is schematized as repeated motifs between cholinergic motor neurons, GABAergic motor neurons, and dorsal and ventral muscles in each body segment (Fig. 1B).

Dorsal muscles and ventral muscles have similar intrinsic excitability Fig. S6. Rhythmic dorsal bending is directly mediated by oscillatory activity of the cholinergic motor neurons within each body segment. Cholinergic motor neurons contract dorsal muscles and simultaneously activate GABAergic neurons that relax ventral muscles. The net effect of dorsal muscle contraction and ventral muscle relaxation is dorsal bending (Fig. 8A, i).

Rhythmic ventral bending is not mediated by its own

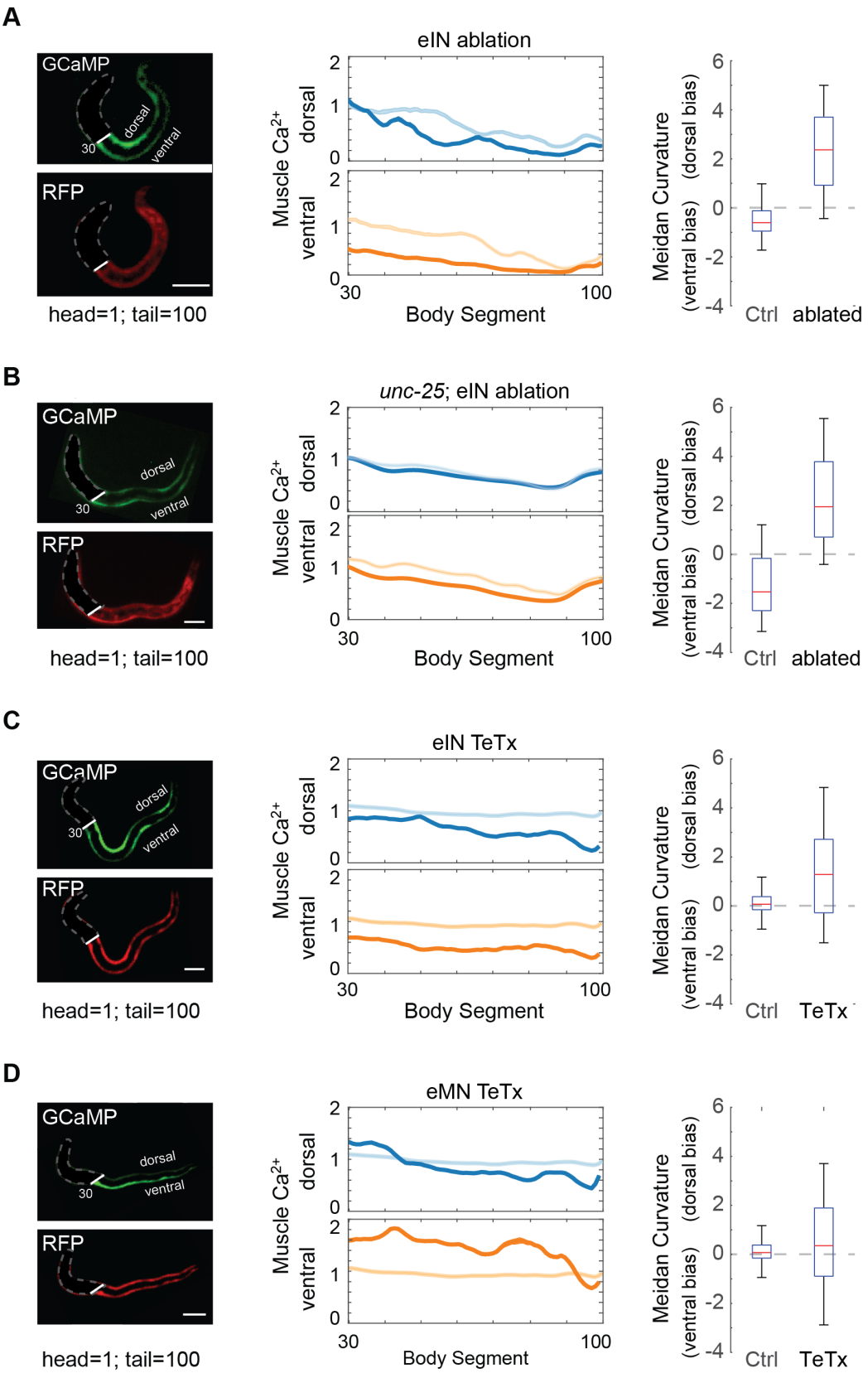

Figure 7. Synaptic transmission from eIN premotor interneurons underline ventral muscle bending A. Example images (left panel), average muscle activity (middle panel), and median body curvature (right panel) of L1 larvae after cholinergic eIN ablation. Average muscle activity for the mock-ablation control group is shown by lighter colored lines (middle panel) and the median body curvature is shown (the right panel). eIN ablation leads to more reduction of ventral muscle activity, resulting in higher dorsal muscle activity; these larvae adopt a crescent shaped posture with a dorsal bias, as evident from the curvature taking a positive value along the body. **B.** Same as **B**, but for mutant L1 larvae without GABA *GAD/unc-25(e156)*. Control group was the mock ablation animals. Upon eIN ablation, larvae again exhibited reduced ventral muscle activity and a dorsal bias in bending. **C.** Example images (left), average calcium activity (middle) and medium body curvature (right) of L1 larvae expressing TeTx in eINs to consecutively block synaptic vesicle releases. Control groups were L1 larvae without TeTx (middle panel, denoted by light-colored lines, and right panels). TeTx expression in eINs resulted in a reduction in ventral muscle activity and a dorsal bias in body bending. **D.** Same as **D**, but with L1 larva expressing TeTx in eMNs. Control groups were L1 larva without TeTx (middle panel, denoted by light-colored lines, and right panels). TeTx expression in eMNs resulted in a higher ventral muscle activity, but not a ventral bias in body bending.

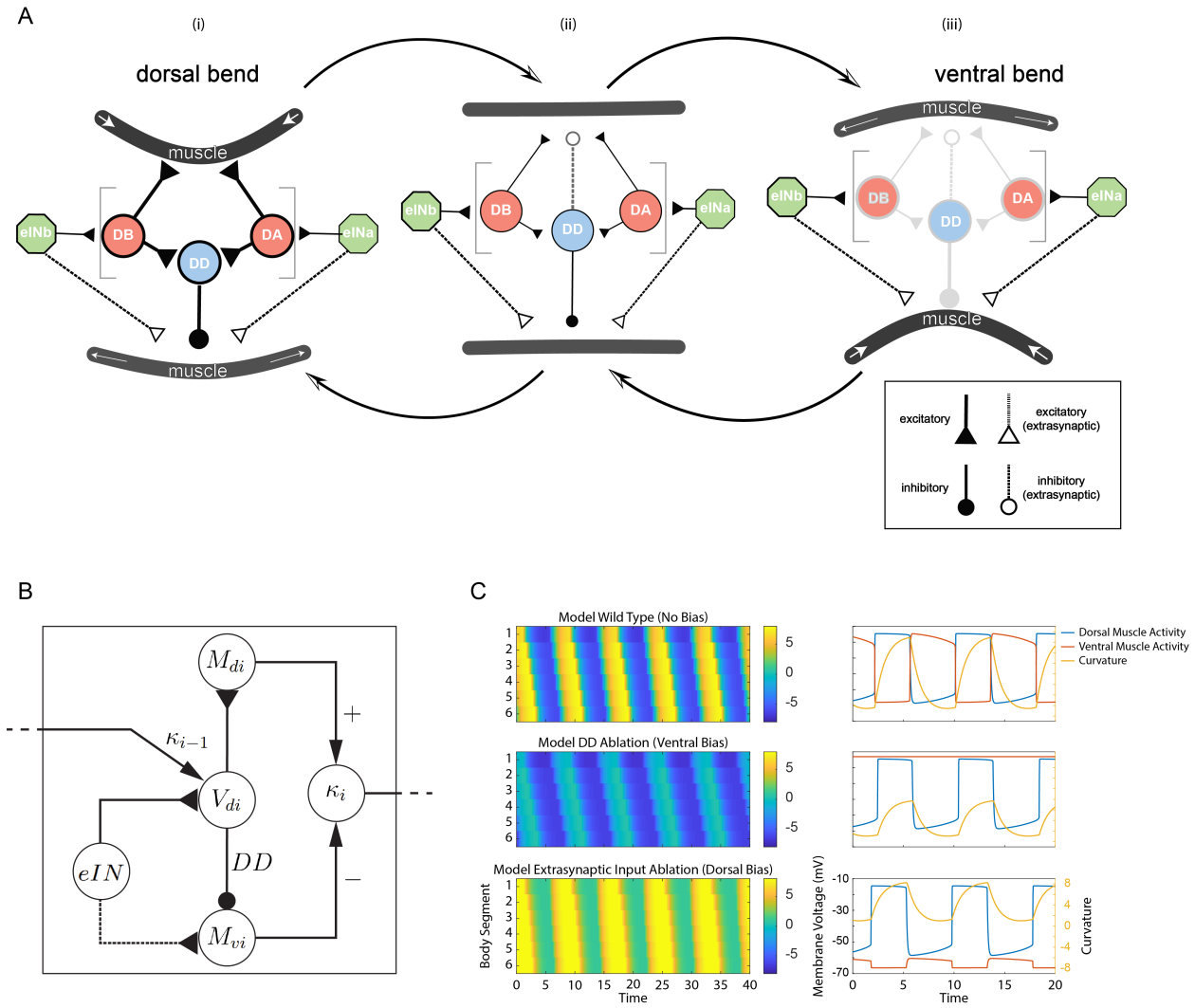

Figure 8. A computational model of the L1 motor circuit A: The L1 larva integrates synaptic transmission and extrasynaptic transmission between premotor interneurons, motor neurons, and muscles, to allow a partial motor circuit to generate alternating dorsal and ventral body bends. Muscles are labelled in yellow, excitatory premotor interneurons (eINs) in red, excitatory motor neurons (DA, DB) in green, inhibitory motor neurons (DD) in blue. Red denotes muscle activities, and the inlet describes wiring for one DA-DB-DD unit and with premotor interneurons. **B:** Schematic of the computational model used to simulate the L1 motor circuit. **C:** (left) Curvature kymographs from the simulation the model circuit for different conditions. (right) Time-series of dorsal and ventral activity along with curvature at mid-body (segment 3). Top row, is the full circuit, which produces traveling waves down the body. Middle row has results from simulation of the circuit with no inhibition, it produces dorsal traveling waves, but no propagating activity on the ventral side, consistent with the *unc-25* animals in Fig. 3. Bottom row simultaion has the extrasynaptic input turned off. In this case, the ventral muscle activity is diminished and there is overall dorsal bias in the bending curvature.

oscillator, but by entrainment to the oscillator that drives dorsal bending. Ventral muscles are uniformly excited by extrasynaptic acetylcholine from premotor interneurons. This permits ventral bends to occur when and where the dorsal oscillator's activity is low (Fig. 8A, iii).

Transition between dorsal bending and ventral bending is also facilitated by negative feedback within each segment: GABA released by inhibitory motor neurons simultaneously relaxes ventral muscles and extrasynaptically inhibits excitatory motor neurons that drive dorsal bending ((Fig. 8A, ii). Thus, in the L1 larva, the same set of motor neurons drives both dorsal and ventral bending. This is in contrast to the adult motor circuit, which has two symmetrically wired motor circuits that separately drive dorsal and ventral bending.

To conceptualize this functional model, we encoded its dynamics in a minimal phenomenological computational model (Fig. 8B) (Methods: Computational model). Similar to work of the adult motor circuit[23], excitatory motor neurons are modeled as an oscillator with calcium and potassium conductances (V_{di}). They provide direct input to dorsal muscles (M_{di}) through an excitatory synapse. Excitatory motor neurons relay a copy of this oscillation to ventral muscles (M_{vi}), inverting its sign through an inhibitory synapse (DD). Because dorsal and ventral muscles have the same resting membrane potential, the inhibitory synapse rectifies dorsal oscillations. This produces alternating dorsal-ventral bends with a deeper dorsal bending (Fig. 8C, lower panel). An extrasynaptic excitatory input to ventral muscles (eIN) alleviates this bias, balancing ventral and dorsal muscle activities (Fig. 8C, upper panel).

We modeled rhythmic bending waves propagating through proprioceptive input between adjacent excitatory motor neurons (κ_i). As in previous models of the adult circuit[23,34], directional wave propagation is encoded by proprioceptive input where the eMN in segment i receives curvature-dependent input from $i-1$ (for forward locomotion) or from $i+1$ (for backward locomotion). Net bending is calculated from the extent of dorsal and ventral muscle

activation in each segment (Methods: Computation model). We tuned parameters by simulating its behaviors to recapitulate key experimental findings (Fig. 7).

Without the inhibitory synapse, this model produces body bending with a stalled wave propagation on the ventral side, which recapitulates the lack of correlation of ventral muscle activity with bending (Fig. 3F). This perturbation generates bending with a strong ventral bias, which was only partially mimicked by the bending behavior of GABA-*unc-25* mutants (Supplementary movie 15). By tuning the extrasynaptic inputs to ventral muscles, this bias can be overcome, which predicts a feedback to premotor interneurons from the downstream circuit. A complete elimination of extrasynaptic input in this model generates dorsal bending across the body, which recapitulates the effect of excitatory premotor interneuron ablation (Fig. 7A-C). Compared to a simpler model where ventral muscles are spontaneously active, an extrasynaptic input to ventral muscles offers more flexibility for bending waves. This functional configuration is an adequate, but likely temporary solution before the development of the larger and more robust adult motor circuit.

Discussion

It is often assumed that symmetric motor circuits are necessary for symmetric motor outputs. *C. elegans* is born only with motor neurons that are wired analogously to the motor subcircuit for dorsal bending in adults. Over the course of larval development, extensive neurogenesis adds the other motor subcircuit for ventral bending, and extensive rewiring eliminates asymmetries in the layout of the newborn circuit.

Yet, the newborn is equally capable of generating adult-like undulatory waves. We show that L1 larva achieves a symmetric gait using the same motor circuit circuitry to drive dorsal bending and to entrain ventral bending. This alternative solution allows newborns to acquire mature gait long before the motor circuit anatomically matures. The larva and adult overcome substantial anatomic differences to generate similar gait; their motor systems have an intrinsic drive to maintain stable output during development.

Extrasynaptic signaling enables an asymmetric L1 motor circuit to generate symmetric motor output

L1 larva's one circuitry solution for symmetric bending requires extrasynaptic signaling at multiple layers of its motor circuit.

Dorsal bending is driven by a configuration that resembles the original half-center model proposed for flexor-extensor coordination during limb movement[1]: synaptic wiring of excitatory and inhibitory motor neurons coordinates dorsal muscle excitation with ventral muscle relaxation. In contrast, ventral bending is generated by entrainment to the rhythmic activity of this dorsal 'half-center'. For this to occur, it is necessary for ventral muscles to be uniformly activated. Acetylcholine from premotor interneurons, which accumulates and acts extrasynaptically, fulfills this role.

Intrinsic oscillatory activities of excitatory motor neurons underlies transitions from dorsal to ventral bending, but GABA release from the inhibitory motor neurons facilitates and modulates this transition. Acting extrasynaptically, this negative feedback inhibits the excitatory motor neurons and promotes dorsal muscles to relax after contraction. With this motor circuit regulating its own exit from dorsal bending and ventral muscles uniformly excited, the rhythmic drop in activity of the dorsal 'half-center' entrains ventral bending. Thus extrasynaptic signaling is necessary for the asymmetric motor circuit to create symmetric output.

Extrasynaptic signaling as an adaptive strategy for a developing motor circuit to create mature behavior

Extrasynaptic signaling is widely observed in invertebrates and vertebrates. Volume transmission of signaling molecules is thought to occur through diffusion, and is thus typically slow and long-lasting[35]. Extrasynaptic accumulation of these signaling molecules may result from either vesicular release at extrasynaptic sites, or by extracellular diffusion of synaptically released neurotransmitters[35]. Our results cannot distinguish between two mechanisms. We favor the diffusion mechanism for extrasynaptic activation of ventral muscles, because we did not observe overt non-synaptic vesicle accumulation in the EM volume of this newborn L1 larva.

Extrasynaptic transmission underlies neuromodulation, allowing hard-wired mature circuits to modify and adapt their output to different contexts. Our results expand the role for extrasynaptic transmission: newly born larvae use it to perform essential signaling that functionally substitutes the requirement for an entire motor subcircuit. As the larva matures, this role is taken over by postembryonically born motor neurons and symmetric synaptic wiring.

Not all extrasynaptic transmission is replaced as the motor circuit matures. Extrasynaptic negative feedback from GABAergic iMN motor neuron to excitatory eMN motor neurons persists in the adult[25–27]. It may be similarly employed in both dorsal and ventral motor subcircuitry.

Extrasynaptic signaling allows the newly born larva to exhibit adult-like gait before its motor circuit is fully developed. Extrasynaptic mechanisms may work particularly well in the larva because of its tiny size. In a short-lived animal, acquiring full mobility at birth is of probable fitness benefit. Extrasynaptic signaling thus represents an adaptive strategy for development.

Neurons adopt new functions to compensate for structural changes of circuits

In small circuits, individual neurons often adopt multiple functions to expand their behavioral repertoires[36,37]. Functional implications of their multi-functional property are generally considered in the context of mature circuits. We show here that neurons also reconfigure their roles across development, to compensate for structural changes that occur during development.

In the adult, cholinergic eMN motor neurons adopt the role of rhythm generation for forward and backward movement. Cholinergic eIN premotor interneurons regulate excitatory eMN motor neurons to switch the output between two modes of locomotion. Our calcium imaging of eIN premotor interneurons and behavioral effect upon their activation (Fig. S7) showed that this role is likely conserved between L1 larva and adult. However, premotor interneurons assume an additional role in the L1 larva: they directly activate ventral muscle cells. This excitation is independent of NMJs from

motor neurons that function downstream of these premotor interneurons; neither is this excitation the consequence of positive feedback from cholinergic motor neurons, because cholinergic motor neurons specifically activated dorsal muscles.

The direct and essential role of premotor interneurons in ventral muscle excitation is likely temporary: ACE, whose enzymatic activity determines extrasynaptic acetylcholine buildup, exhibits dorsal-ventral asymmetry in the new born larva. Asymmetry disappears in adults, coinciding with emergence of ventral muscle-innervating motor neurons of the adult circuit[38]. Thus, a neuron's flexibility to adopt multiple roles also provides a means to compensate for a circuit's developmental immaturity. In L1 larvae, it allows mature motor patterns to emerge before the completion of motor circuit development.

Circuit degeneracy maintains an animal's motor patterns

Our study presents a profound example of circuit degeneracy: dissimilar circuits generate similar behaviors. Indeed, one functional output can have multiple network solutions by correlated changes in the properties of neurons and synapses[39]. Examples of circuit degeneracy include similar motor patterns exhibited by two mollusk subspecies with substantial differences in electrical connectivity[40], and maintenance of a pyloric circuit's output at different temperatures by varying parameters of many synaptic connectivity[41].

We show that degenerate mechanisms constitute adaptive strategies to minimize functional disruption during development. Throughout postnatal development *C. elegans* generates an undulatory motor pattern even while the larva undergoes substantial growth in body size, neurite extension, neurogenesis, and synapse-rearrangement. To maintain a stable motor output during anatomic development likely represents an intrinsic drive in response to ecological demand.

An adequate but temporary solution for a developing motor circuit

Our computational model imposes that bending originates from oscillations of dorsal excitatory motor neurons, which entrains ventral muscles. Propagation of bending waves is contingent on proprioceptive input from neighboring segments, and different strengths of synaptic and extrasynaptic inputs from premotor interneurons. An implication of this model is that synaptic input to dorsal but not ventral muscle dictates L1's wave propagation. Indeed, we noted that when we perturbed synaptic input to dorsal and ventral muscles, changes in dorsal muscle's calcium dynamics correlated with bending pattern changes, whereas ventral muscle's calcium dynamics could not predict bending (Supplemental movie 14).

An early theoretical model of the L1 motor circuit[42] assumes that ventral muscles are spontaneously active and predicts that inhibitory neurons are essential for forward locomotion. Both contradict our experimental observations. In a model that fits the motor dynamics of the L1 larva, ventral muscles are kept active through extrasynaptic excitatory input. It offers more flexibility for bending waves because dorsal and ventral bending can be precisely tuned by different strengths of synaptic and extrasynaptic inputs from premotor interneurons. In this model, dorsal and ventral bending activity is balanced within a small space of tuned parameters, which makes bending symmetry susceptible to perturbation. This configuration offers an adequate but temporal solution for the developing larva.

Methods

Constructs, transgenes and strains

A list of constructs, transgenic arrays, and transgenic strains acquired and generated for this study is summarized in the Supplemental text.

Electron microscopy of L1 larvae

Serial section SEM and TEM was performed as previously described[43,44]. Briefly, L1 larvae were high pressure frozen, freeze substituted, embedded in resin, serial sectioned at 30 or 50nm thickness, and imaged at approximately 1nm/pixel. Images were stitched into 3D volumes using TrakEM2[45], a Fiji plugin[46], and annotated using skeleton tracing in CATMAID[47].

Synchronization of young L1 larvae

Young L1 larvae used for most behavioral and imaging experiments were collected as follows. On the day of experiment, up to fifty 3-fold stage eggs from plates with well-fed gravid adults were transferred to a new plate seeded with OP50. Eggs were allowed to hatch for 1hr at 22.5°C and unhatched eggs were removed. All experiments were carried out within 5-6 hours afterwards to ensure that they have not integrated post-embryonically derived motor neurons.[13].

Crawling assays and analyses

Free crawling on culturing plates For most recordings (Fig. 7), individual L1 larvae hatched on a thin lawn of OP50 on a NGM plate (above) were recorded directly from the plate using a dissecting microscope (Zeiss V16). Some recording were performed using a customized wide-field compound microscope[15] with larva movements manually tracked during recording. For some experiments, larvae were maintained until adulthood to verify successful ablation of neurons (Fig. 7A-D).

Imaging analyses were carried out using in-house MATLAB scripts to analyze both body angle and velocity. Orientation (head, tail, ventral, and dorsal) were manually assigned in the first frame of the recording and tracked automatically afterwards. Contours of L1 larva were segmented and divided into 100 segments along the anterior-posterior axis, and errors fixed by manual curation. This program outputs angles at each segment and displacement at each joint.

On plate optogenetic stimulation These experiments were applied to animals that express opsins. For each set of experiments, the control and experimental group contained animals of the same genotype, with the control group cultured on plates without all-trans retinal (ATR)[48]. Recording was done per individual larva, on the same, unseeded plate that did not have ATR for each experimental group.

For the experimental group, individual L1 larva from parents incubated on the NMG plates seeded with the OP50 culture in 0.1mg/ml ATR for at least two generations was picked onto an unseeded NMG plate without ATR, and recorded as described above, typically for 75sec at 26Hz. The control group was

recorded on another unseeded plate to avoid ATR cross-contamination.

Both experimental and control groups were subjected to the same optogenetic stimulation from a LED light source controlled by a customized ImageJ[49] plugin via Arduino[15]. The stimulation protocol was 10 second light-off (pre-stimulation), 4 consecutive epoches of stimulation consisting of 10 second light-on and 5 second light-off, followed by 10 second light-off (post-stimulation). Image analyses were carried out using customized MATLAB scripts. The light-on and light-off phases were automatically annotated by light intensity of the image.

Swimming assays

Recording of wildtype L1 larva swimming (Fig. 1) was performed in a miniature well fabricated using polydimethylsiloxane in Hang Lu lab (Georgia Institute of Technology, USA). A droplet of M9 was mounted onto the center of the well and a L1 larva was transferred into the M9 droplet. With a coverslip mounted, this swimming pool was placed on a glass slide and recorded with a 4x objective using the same setup as described above, typically for 68sec at 26Hz. Body postures were manually scored frame-by-frame. Ventral side of the larva were manually identified by the presence of anus and/or the gonad. A dorsal-biased bending posture (D) was defined by a convex towards the dorsal side from the neck (30%) to the tail. A ventral-biased bending posture (V) was defined by a convex towards the ventral side from the neck (30%) to the tail. All other postures were counted as 'intermediate'. Frames where neither the anus nor the gonad could be confidently identified were discarded. The total number of frames one larva spent in one of the three postures was normalized against the total number of frames for each recording.

Photo-ablation by miniSOG

Transgenic animals that express blue-light activated miniSOG protein were used in these experiments, performed and verified as described[22]. Briefly, to visually examine ablation efficiency, miniSOG was co-expressed with SL2-RFP to tag the to-be-ablated neurons and neurites. Young larvae were picked to be exposed to blue LED light. Cells that activated apoptosis usually appear vacuolar shortly after the light treatment. But the complete disappearance of soma and neurites could only be observed towards the end of the larval stage.

A home-made chamber, designed and made by Taizo Kawano and Thomas Sun (LTRI), delivers the blue LED light, dissipates heat and supplies oxygen by electrical fan ventilation during illumination. For each experiment, 1hr post-hatching larvae on a seeded plate were placed in the chamber upright with its lid removed. The optimal exposure time was experimentally determined for each strain to ablate cells without arresting larva growth. The eIN ablation strain required 30 minute exposure at the closest distance to the light of the plate holder. After illumination, the plate was covered and kept in darkness for 4 hours, before subjecting animals to subsequent behavioral and calcium imaging experiments.

After each larva was imaged, it was recovered and transferred onto individual plates to allow growing for 2 days. They were examined again, and only data recorded from those with absence of RFP markers in labelled neurons were used for analyses.

Calcium imaging of neurons

Recordings were performed using a customized LED-powered wide-field tracking compound microscope. Transgenic strains expressing genetic calcium sensor GCaMP6s fused with RFP and dual-color recording was performed with an in-house developed ImageJ plugin as described previously[15,50].

L1 larvae crawling on agarose pads were recorded. L1 larvae were placed into a droplet of M9 or halocarbon oil on a 2% agarose pad and mounted by a coverslip. We adjusted The amount of M9 (or using halocarbon oil) to reduce crawling speed of L1 larvae, which help reducing motion artifacts. For M9, most liquid needs to be absorbed before placing the coverslip. For halocarbon oil, the coverslip can be directly applied when the oil droplet was still spreading.

Recordings were typically performed with 40x or 63x objectives, at 10Hz or 26Hz, for 68s or 90s. Tracking was typically performed manually with a joystick that controls the motorized stage. Tracking of ROIs were performed with a MATLAB script modified from[51]. After manual curation of automated tracking, the script outputs fluorescent intensity and displacement to allow calculation of calcium dynamics, velocity and bending angles.

Calcium imaging of muscles

Larvae expressing GCaMP3 and tagRFP separately in body wall muscles are used in this experiment. Some Recordings (Fig.1D) were performed on L1 larvae crawling slowly on agarose pads, using the same setup for neuronal calcium imaging as above. Other recordings (Fig.7A-D) were performed on unconstrained L1 larvae on unseeded NGM plates, using a Nikon scanning microscope operating in a wide-field mode.

Post-imaging analyses were performed using a customized MATLAB-based pipeline for muscle segmentation and signal processing. This program requires user input to determine the head and tail in the first frame of the recording. It isolates the contour of muscles, and divided it into 100 segments along the anterior-posterior axis. They were further segment into the dorsal and ventral segments along the midline. The average value for pixels within each segment is used as proxy for the activity for this muscle segment. Angles formed by intersecting vectors are calculated.

A simple strategy for simultaneous optogenetic stimulation and calcium imaging

All-optical interrogation of neural circuit has been a technical challenge, largely due to the overlapping excitation spectra between most potent opsins and the most popular genetic calcium sensor GCaMP[52]. Two general strategies have been adopted to circumvent this issue. First is to spatially separated pattern illumination[52,53]. Second is to spectrally separate opsin stimulation and activity recording[53–58].

Here we achieve all-optical interrogation without sophisticated setups. Because of the latency in the change of intracellular calcium level, and the response of genetic calcium reporters upon optogenetic perturbation of neuronal activity, and the sensitivity of opsins, we can apply the initial response of genetic calcium sensor, which simulatenously activate opsins, to examine the effect of optogenetic perturbation of

neuronal activity.

We validated this approach with a characterized connection (cholingeric motor neurons to their downstream GABAergic motor neurons), and applied it for examination of a complete motor circuit. This protocol conducts bi-directional (activation and inhibition) all-optical interrogation with any combination between all tested opsins (ChR2, Chrimson, Halorodopsin, GtACR2) and genetic calcium sensors (GCaMP and cameleon) (this study and data not shown). It can be carried out on even conventional wide-field fluorescent microscopy setup.

Obviously, this method has limited capacity to provide information on dynamic properties of the connections. But the practicality of this experimental protocol makes it feasible and generally applicable first-step establishment of the causative, functional connections of a neural circuit.

To carry out all-optical interrogation, strains that express opsins in upstream cells and calcium sensors in downstream cell were cultured on ATR-supplemented plates. A control group was cultured on plates without all-trans retinal. On day of experiment, synchronize L1 larvae of the crossed strain. For ATR experimental group, particularly strains generated from the Cre-loxP system, larvae grown on 2x or 4x concentration of regular ATR plate (250μM ATR) for multiple generations were ideal to maximize the strength of optogenetic stimulation. L1 larvae were mounted on slides with limited M9 solution for immobilization. Imaging was performed as described for neuron calcium imaging. After one minute after samples were mounted on slides, without turning on the LED light source, recording was carried out at 10Hz-26Hz. The LED stimulation/calcium imaging light was turned on and off during recording, with an on phase usually lasted longer than 3 seconds, and off phase between 5-20 seconds. Randomness was intentional, as this approach should randomize the initial activity state of both the cells being manipulated and recorded. Once the recording was completed, either repeat the recording on the same larva or another larva. Calcium imaging analyses were carried out as described. Typically only the first 3-6 second recording for each epoch was used for analyses. We noticed established transgenic lines exhibited varying degrees of transient leaky expression in L1 body wall muscles; strains that use the Cre-LoxP system to further restrict expression included those that was used for cholinergic motor neuron inhibition and premotor interneurons inhibition.

A computational model

We modeled each segment of L1 circuit using the equations below (1-5), which was schematized in Fig. 8B. The model is inspired by the Morris-Lecar model of the Barnacle giant muscle fiber[59]. It's a reduced order nonlinear model with an instantaneous calcium current, a potassium current with an activation variable, and a passive leak current. A similar model was used previously to study adult *C. elegans* locomotion[23]. We model 6 segments coupled to each other proprioceptively, corresponding to the 6 DD neurons.

$$C_m \frac{dV_{di}}{dt} = -g_L(V_{di}-E_L) - g_{Ca} m_\infty(V_{di})(V_{di}-E_{Ca}) - g_K n_{di}(V_{di}-E_K) + c\kappa_{i-1} + I_{SYN+}^{V_{eIN}} \quad (1)$$

$$\tau_n \frac{dn_{di}}{dt} = -n_{di} + n_\infty(V_{di}) \quad (2)$$

$$\tau_u \frac{dM_{di}}{dt} = -M_{di} + I_{SYN+}^{V_{di}} \quad (3)$$

$$\tau_u \frac{dM_{vi}}{dt} = -M_{vi} + I_{SYN-}^{V_{di}} + I_{SYN\star}^{V_{eIN}} \quad (4)$$

$$\tau_b \frac{d\kappa_i}{dt} = -\kappa_i + \sigma(M_{di}) - \sigma(M_{vi}) \quad (5)$$

Where, $E_L = -60$ mV, $E_{Ca} = 60$ mV, $E_K = -70$ mV are the leak, calcium and potassium reversal potentials respectively. Terms $g_L = 100$ pS, $g_{Ca} = 400$ pS, $g_K = 500$ pS are the maximal leak, calcium and potassium conductances and $C_m = 3$ pF is the membrane capacitance. Timescale parameters were set as $\tau_n = 30$ ms, $\tau_u = 85$ ms, $\tau_b = 10$ ms The function $m_\infty(V) = \frac{1}{1+\exp\left(\frac{V_m - V}{\theta_m}\right)}$ with $\theta_m = 10.25$ mV, $V_m = -29$ mV. And $n_\infty(V) = \frac{1}{1+\exp\left(\frac{V_n - V}{\theta_n}\right)}$ with $\theta_n = 20$ mV, $V_n = -55$ mV. While, $\sigma(V) = \alpha(\tanh(\beta * V) + 1)$ with $\beta =$ and $\alpha = 1000$ and $\beta = 0.01$ converts muscle activities into curvature.
The terms $I_{SYN+}^{V_{eIN}}$, $I_{SYN-}^{V_{di}}$, $I_{SYN\star}^{V_{eIN}}$, respectively are the synaptic currents from the excitatory synapse from eMN to dorsal muscles, the inhibitory synapse from eMN to ventral muscles, and the excitatory extrasynaptic input from eIN to ventral muscles. The synaptic currents are based on the graded synapse model used in[60], and are defined as follows.

$$I_{SYN+}^{V_{eIN}} = g(V_{di})(M_{di} - E^+)$$
$$I_{SYN-}^{V_{di}} = g(V_{di})(M_{vi} - E^-)$$
$$I_{SYN\star}^{V_{eIN}} = g(V_{eIN})(M_{vi} - E^\star)$$
$$g(V) = \frac{\bar{g}}{1+\exp\{K\left(\frac{V_k - V}{V_{range}}\right)\}}$$

With $K = 2\ln(\frac{0.1}{0.9})$, set such that the conductance varied from 10% to 90% of its maximum value over the presynaptic voltage range set by V_{range}. Other parameters were set as $\bar{g} = 1$ nS, $V_k = -30$ mV, $V_{range} = 20$. Terms $E^+, E^-, E^\star$ are the reversal potentials for the excitatory receptor, inhibitory receptor and the extrasynaptic receptor. We set $E^+ = -10$ mV. E^- and $E^\star$ were treated as variables and optimized to result in an unbiased gait, such that the mean value of the bending curvature $\langle \kappa_i \rangle$ is zero. The optimized values were found to be $E^- = -67$ mV, $E^\star = 33.5$ mV.

MATLAB scripts

MATLAB scripts developed for behavioral, neuronal and muscle calcium imaging analyses are available in GitHub https://github.com/zhen-lab/Beta_Function_Analysis

ACKNOWLEDGEMENTS
We thank Taizo Kawano, Ying Wang, Jin Meng, Yan Li and Thomas Sun for technical support; lab members of Mei Zhen, Shangbang Gao and Aravinthan Samuel for discussions; Albert Cardona and Andrew Chisholm for guidance on the CATMAID server and cell identification. This work was supported by the International Human Frontier Science Program Organization RGP0051/2014 and the Canadian Institutes of Health Research Foundation Scheme 154274.

AUTHOR CONTRIBUTIONS
MZ and QW conceived the project; MZ supervised the project; YL, TA, AG, BM, WH, JM and MZ designed and performed experiments and analyzed data. DW and BM performed EM reconstruction; TA developed model; YL, TA and QW developed scripts. YL, TA, ADTS, MZ wrote the paper. All authors read or edited the paper.

COMPETING INTERESTS
The authors declare no competing interests.

References

[1] Thomas Graham Brown. "Studies in the physiology of the nervous system. XXVIII: Absence of algebraic equality between the magnitudes of central excitation and effective central inhibition given in the reflex centre of a single limb by the same reflex stimulus." In: *Quarterly Journal of Experimental Physiology: Translation and Integration* 14.1 (1924), pp. 1–23.

[2] Thomas Graham Brown. "The intrinsic factors in the act of progression in the mammal". In: *Proceedings of the Royal Society of London. Series B, containing papers of a biological character* 84.572 (1911), pp. 308–319.

[3] Ole Kiehn. "Decoding the organization of spinal circuits that control locomotion". In: *Nature Reviews Neuroscience* 17.4 (2016), p. 224.

[4] Ole Kiehn. "Locomotor circuits in the mammalian spinal cord". In: *Annu. Rev. Neurosci.* 29 (2006), pp. 279–306.

[5] Heekyung Jung and Jeremy S Dasen. "Evolution of patterning systems and circuit elements for locomotion". In: *Developmental cell* 32.4 (2015), pp. 408–422.

[6] Catarina Catela, Maggie M Shin, and Jeremy S Dasen. "Assembly and function of spinal circuits for motor control". In: *Annual Review of Cell and Developmental Biology* 31 (2015), pp. 669–698.

[7] JG White, DG Albertson, and MAR Anness. "Connectivity changes in a class of motoneurone during the development of a nematode". In: *Nature* 271.5647 (1978), p. 764.

[8] John G White, Eileen Southgate, and J Nichol Thomson. "The structure of the nervous system of the nematode Caenorhabditis elegans". In: (1986).

[9] Janet E Richmond and Erik M Jorgensen. "One GABA and two acetylcholine receptors function at the C. elegans neuromuscular junction". In: *Nature neuroscience* 2.9 (1999), pp. 791–797.

[10] Shangbang Gao and Mei Zhen. "Action potentials drive body wall muscle contractions in Caenorhabditis elegans". In: *Proceedings of the National Academy of Sciences* 108.6 (2011), pp. 2557–2562.

[11] Ping Liu et al. "Genetic dissection of ion currents underlying all-or-none action potentials in C. elegans body-wall muscle cells". In: *The Journal of physiology* 589.1 (2011), pp. 101–117.

[12] John Edward Sulston. "Post-embryonic development in the ventral cord of Caenorhabditis elegans". In: *Philosophical Transactions of the Royal Society of London. B, Biological Sciences* 275.938 (1976), pp. 287–297.

[13] John E Sulston and H Robert Horvitz. "Post-embryonic cell lineages of the nematode, Caenorhabditis elegans". In: *Developmental biology* 56.1 (1977), pp. 110–156.

[14] Martin Chalfie et al. "The neural circuit for touch sensitivity in Caenorhabditis elegans". In: *Journal of Neuroscience* 5.4 (1985), pp. 956–964.

[15] Taizo Kawano et al. "An imbalancing act: gap junctions reduce the backward motor circuit activity to bias C. elegans for forward locomotion". In: *Neuron* 72.4 (2011), pp. 572–586.

[16] Nathan C Klapoetke et al. "Independent optical excitation of distinct neural populations". In: *Nature methods* 11.3 (2014), pp. 338–346.

[17] Elena G Govorunova et al. "Natural light-gated anion channels: A family of microbial rhodopsins for advanced optogenetics". In: *Science* 349.6248 (2015), pp. 647–650.

[18] Yehezkel Ben-Ari. "Excitatory actions of gaba during development: the nature of the nurture". In: *Nature Reviews Neuroscience* 3.9 (2002), p. 728.

[19] Bingjie Han, Andrew Bellemer, and Michael R Koelle. "An evolutionarily conserved switch in response to GABA affects development and behavior of the locomotor circuit of Caenorhabditis elegans". In: *Genetics* 199.4 (2015), pp. 1159–1172.

[20] Mei Zhen and Aravinthan DT Samuel. "C. elegans locomotion: small circuits, complex functions". In: *Current opinion in neurobiology* 33 (2015), pp. 117–126.

[21] Yingchuan B Qi et al. "Photo-inducible cell ablation in Caenorhabditis elegans using the genetically encoded singlet oxygen generating protein miniSOG". In: *Proceedings of the National Academy of Sciences* 109.19 (2012), pp. 7499–7504.

[22] Shangbang Gao et al. "Excitatory motor neurons are local oscillators for backward locomotion". In: *Elife* 7 (2018), e29915.

[23] Tianqi Xu et al. "Descending pathway facilitates undulatory wave propagation in Caenorhabditis elegans through gap junctions". In: *Proceedings of the National Academy of Sciences* 115.19 (2018), E4493–E4502.

[24] Anthony D Fouad et al. "Distributed rhythm generators underlie Caenorhabditis elegans forward locomotion". In: *Elife* 7 (2018), e29913.

[25] Christian Schultheis et al. "Optogenetic analysis of GABAB receptor signaling in Caenorhabditis elegans motor neurons". In: *Journal of neurophysiology* 106.2 (2011), pp. 817–827.

[26] Yu Shen et al. "An extrasynaptic GABAergic signal modulates a pattern of forward movement in Caenorhabditis elegans". In: *Elife* 5 (2016), e14197.

[27] Jeremy S Dittman and Joshua M Kaplan. "Behavioral impact of neurotransmitter-activated G-protein-coupled receptors: muscarinic and GABAB receptors regulate Caenorhabditis elegans locomotion". In: *Journal of Neuroscience* 28.28 (2008), pp. 7104–7112.

[28] Christelle Gally and Jean-Louis Bessereau. "GABA is dispensable for the formation of junctional GABA receptor clusters in Caenorhabditis elegans". In: *Journal of Neuroscience* 23.7 (2003), pp. 2591–2599.

[29] Berangere Pinan-Lucarre et al. “C. elegans Punctin specifies cholinergic versus GABAergic identity of postsynaptic domains”. In: *Nature* 511.7510 (2014), pp. 466–470.

[30] Laura Pereira et al. “A cellular and regulatory map of the cholinergic nervous system of C. elegans”. In: *Elife* 4 (2015), e12432.

[31] Sean T Sweeney et al. “Targeted expression of tetanus toxin light chain in Drosophila specifically eliminates synaptic transmission and causes behavioral defects”. In: *Neuron* 14.2 (1995), pp. 341–351.

[32] Evan L Ardiel et al. “Visualizing calcium flux in freely moving nematode embryos”. In: *Biophysical journal* 112.9 (2017), pp. 1975–1983.

[33] Richard Michael Durbin. *Studies on the development and organisation of the nervous system of Caenorhabditis elegans*. 1987.

[34] Jordan Hylke Boyle, Stefano Berri, and Netta Cohen. “Gait modulation in C. elegans: an integrated neuromechanical model”. In: *Frontiers in computational neuroscience* 6 (2012), p. 10.

[35] Citlali Trueta and Francisco Fernandez De-Miguel. “Extrasynaptic exocytosis and its mechanisms: a source of molecules mediating volume transmission in the nervous system”. In: *Frontiers in physiology* 3 (2012), p. 319.

[36] Peter A Getting. “Emerging principles governing the operation of neural networks”. In: *Annual review of neuroscience* 12.1 (1989), pp. 185–204.

[37] Kevin L Briggman and WB Kristan Jr. “Multifunctional pattern-generating circuits”. In: *Annu. Rev. Neurosci.* 31 (2008), pp. 271–294.

[38] Didier Combes et al. “Multiple ace genes encoding acetylcholinesterases of Caenorhabditis elegans have distinct tissue expression”. In: *European Journal of Neuroscience* 18.3 (2003), pp. 497–512.

[39] Eve Marder, Marie L Goeritz, and Adriane G Otopalik. “Robust circuit rhythms in small circuits arise from variable circuit components and mechanisms”. In: *Current opinion in neurobiology* 31 (2015), pp. 156–163.

[40] Akira Sakurai and Paul S Katz. “Artificial synaptic rewiring demonstrates that distinct neural circuit configurations underlie homologous behaviors”. In: *Current Biology* 27.12 (2017), pp. 1721–1734.

[41] Timothy O’Leary and Eve Marder. “Temperature-robust neural function from activity-dependent ion channel regulation”. In: *Current Biology* 26.21 (2016), pp. 2935–2941.

[42] Jordan H Boyle and Netta Cohen. “A minimal model of C. elegans forward locomotion: the larval L1 circuit”. In: *BMC Neuroscience* 12.1 (2011), pp. 1–1.

[43] Ben Mulcahy et al. “A pipeline for volume electron microscopy of the Caenorhabditis elegans nervous system”. In: *Frontiers in neural circuits* 12 (2018), p. 94.

[44] Daniel Witvliet et al. “Connectomes across development reveal principles of brain maturation”. In: *Nature* (2021), pp. 1–5.

[45] Albert Cardona et al. “TrakEM2 software for neural circuit reconstruction”. In: *PloS one* 7.6 (2012), e38011.

[46] Johannes Schindelin et al. “Fiji: an open-source platform for biological-image analysis”. In: *Nature methods* 9.7 (2012), pp. 676–682.

[47] Stephan Saalfeld et al. “CATMAID: collaborative annotation toolkit for massive amounts of image data”. In: *Bioinformatics* 25.15 (2009), pp. 1984–1986.

[48] Georg Nagel et al. “Light activation of channelrhodopsin-2 in excitable cells of Caenorhabditis elegans triggers rapid behavioral responses”. In: *Current Biology* 15.24 (2005), pp. 2279–2284.

[49] Caroline A Schneider, Wayne S Rasband, and Kevin W Eliceiri. “NIH Image to ImageJ: 25 years of image analysis”. In: *Nature methods* 9.7 (2012), pp. 671–675.

[50] Maria A Lim et al. “Neuroendocrine modulation sustains the C. elegans forward motor state”. In: *Elife* 5 (2016), e19887.

[51] Quan Wen et al. “Proprioceptive coupling within motor neurons drives C. elegans forward locomotion”. In: *Neuron* 76.4 (2012), pp. 750–761.

[52] Zengcai V Guo, Anne C Hart, and Sharad Ramanathan. “Optical interrogation of neural circuits in Caenorhabditis elegans”. In: *Nature methods* 6.12 (2009), p. 891.

[53] John Peter Rickgauer, Karl Deisseroth, and David W Tank. “Simultaneous cellular-resolution optical perturbation and imaging of place cell firing fields”. In: *Nature neuroscience* 17.12 (2014), p. 1816.

[54] Jasper Akerboom et al. “Genetically encoded calcium indicators for multi-color neural activity imaging and combination with optogenetics”. In: *Frontiers in molecular neuroscience* 6 (2013), p. 2.

[55] Christina K Kim et al. “Simultaneous fast measurement of circuit dynamics at multiple sites across the mammalian brain”. In: *Nature methods* 13.4 (2016), p. 325.

[56] Adam M Packer et al. “Simultaneous all-optical manipulation and recording of neural circuit activity with cellular resolution in vivo”. In: *Nature methods* 12.2 (2015), p. 140.

[57] Priyamvada Rajasethupathy et al. “Projections from neocortex mediate top-down control of memory retrieval”. In: *Nature* 526.7575 (2015), p. 653.

[58] Zihui Zhang et al. “Closed-loop all-optical interrogation of neural circuits in vivo”. In: *Nature methods* 15.12 (2018), pp. 1037–1040.

[59] Catherine Morris and Harold Lecar. “Voltage oscillations in the barnacle giant muscle fiber”. In: *Biophysical journal* 35.1 (1981), pp. 193–213.

[60] Stephen R Wicks, Chris J Roehrig, and Catharine H Rankin. “A dynamic network simulation of the nematode tap withdrawal circuit: predictions concerning synaptic function using behavioral criteria”. In: *Journal of Neuroscience* 16.12 (1996), pp. 4017–4031.

[61] Cornelia Schmitt et al. “Specific expression of channelrhodopsin-2 in single neurons of Caenorhabditis elegans”. In: *PloS one* 7.8 (2012).

[62] Victoria J Butler et al. “A consistent muscle activation strategy underlies crawling and swimming in Caenorhabditis elegans”. In: *Journal of the Royal Society Interface* 12.102 (2015), p. 20140963.

Supplemental figures

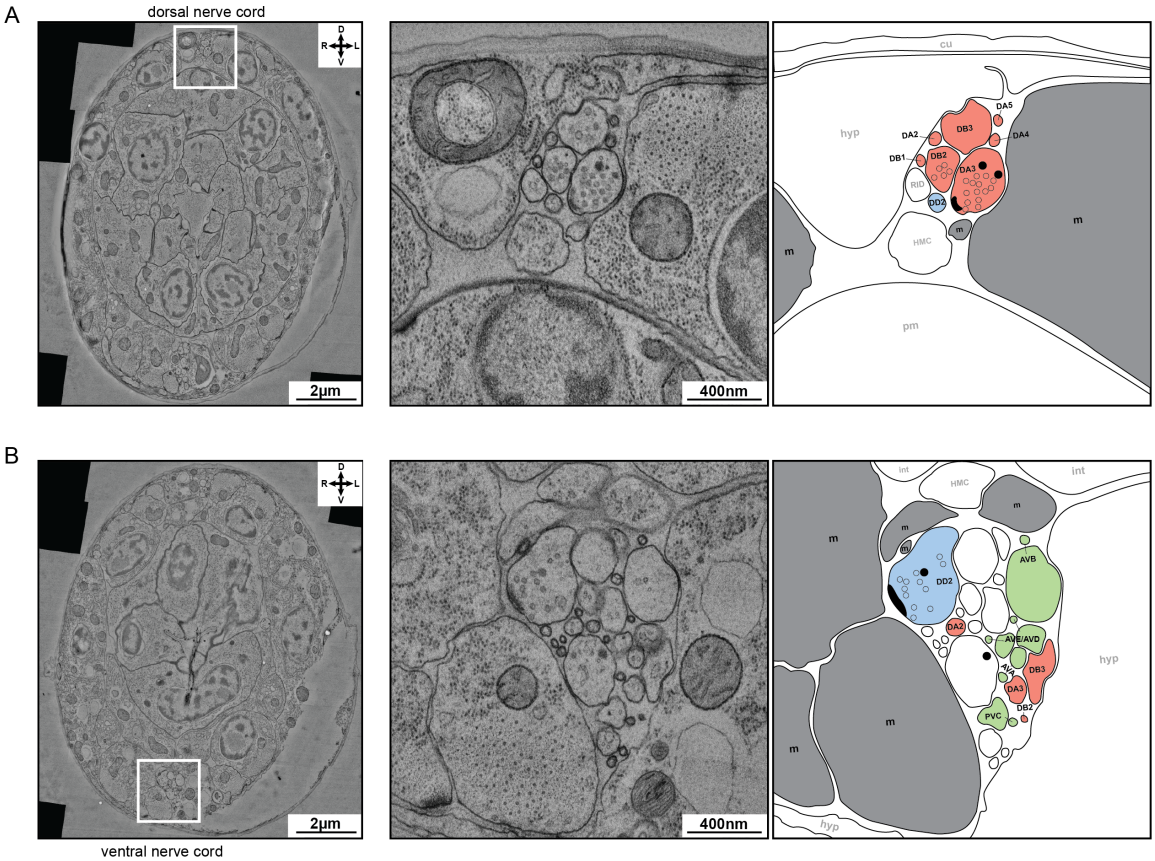

Figure S1. Electron microscopy reconstructions of the ventral and dorsal nerve cord of an 5-6hr L1 larvae. **A.** An example image of the dorsal nerve cord. *(Left)* An electron micrograph of the cross-section of the L1 larva, where its dorsal nerve cord was marked by a white box. *(Center)* An enlarged view of images inside the white box, where cross-sections of individual neurites of the L1 motor circuit neurons and muscles were color-coded and named with dark letters *Right*. Red: eMNs; blue:iMNs; grey: muscles. One eMN (DA3) makes a dyatic synapse to the muscle and iMN (DD2); its presynpatic terminal contains an active zone (black crescent), synaptic vesicles (clear circles) and dense core vesicles (dark circles). **B.** An example image of the ventral nerve cord annotation, similarly illustrated and annotated as in A. Neurites for eIN, which are absent from the dorsal nerve cord (A), are color-coded green. An iMN (DD2) makes a NMJ to muscles. *Right panels:* Cross-sections of other neuron (RID) and cell (HMC) of the L1 motor circuit in the dorsal (A) and ventral (B) cords (B) were labelled by opaque letters. *Abbreviations:* m: muscle; pm: pharyngeal muscle; hyp: hypodermis; cu: cuticle; int: intestine.

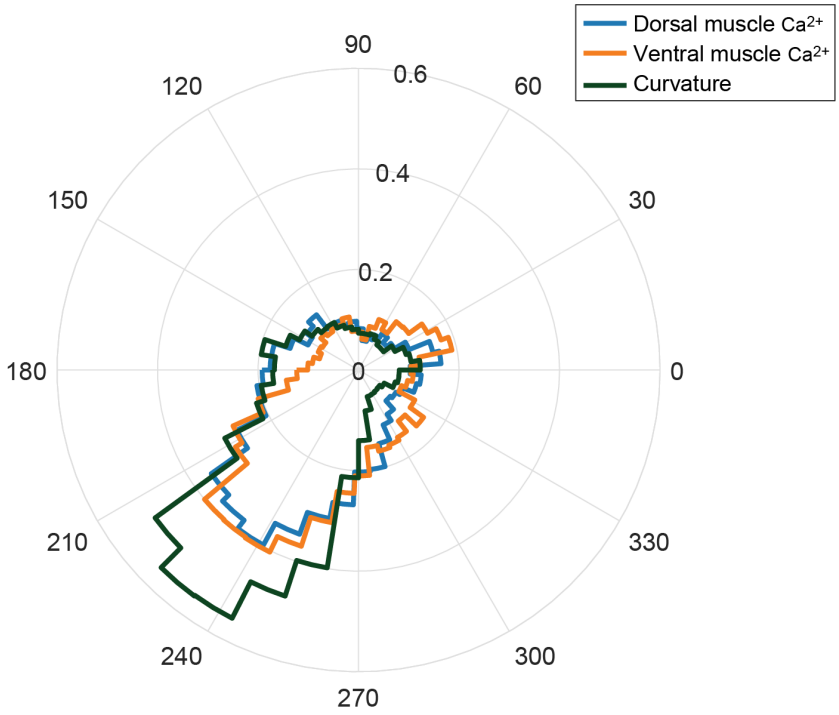

Figure S2. Polar histogram of phase differences between the propagation of dorsal muscle calcium, ventral muscle calcium, and body bending. Under this imaging condition (Fig. 1E), L1 larvae were allowed to crawl very slowly. The speed of bending propagation is similar to that of calcium signal (GCaMP3) propagation in both dorsal and ventral muscles.

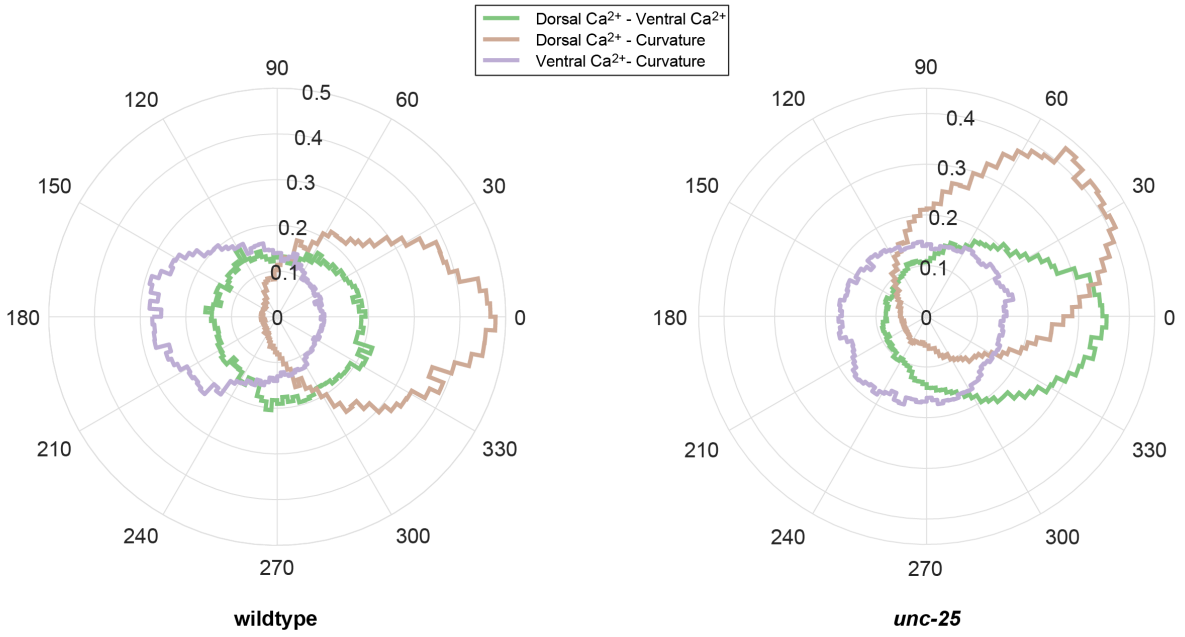

Figure S3. Only dorsal muscle calcium dynamics exhibits correlation with bending in *unc-25* mutant L1 larva. Polar histograms of muscle calcium imaging of crawling wildtype (left) and *unc-25 right* L1 larva under the same imaging condition. *Left* In wildtype larva, both dorsal and ventral muscles exhibit correlation with bending that was anti-phasic to each other. *Right* In *unc-25* larva, dorsal but not ventral muscles exhibited correlation with the bending.

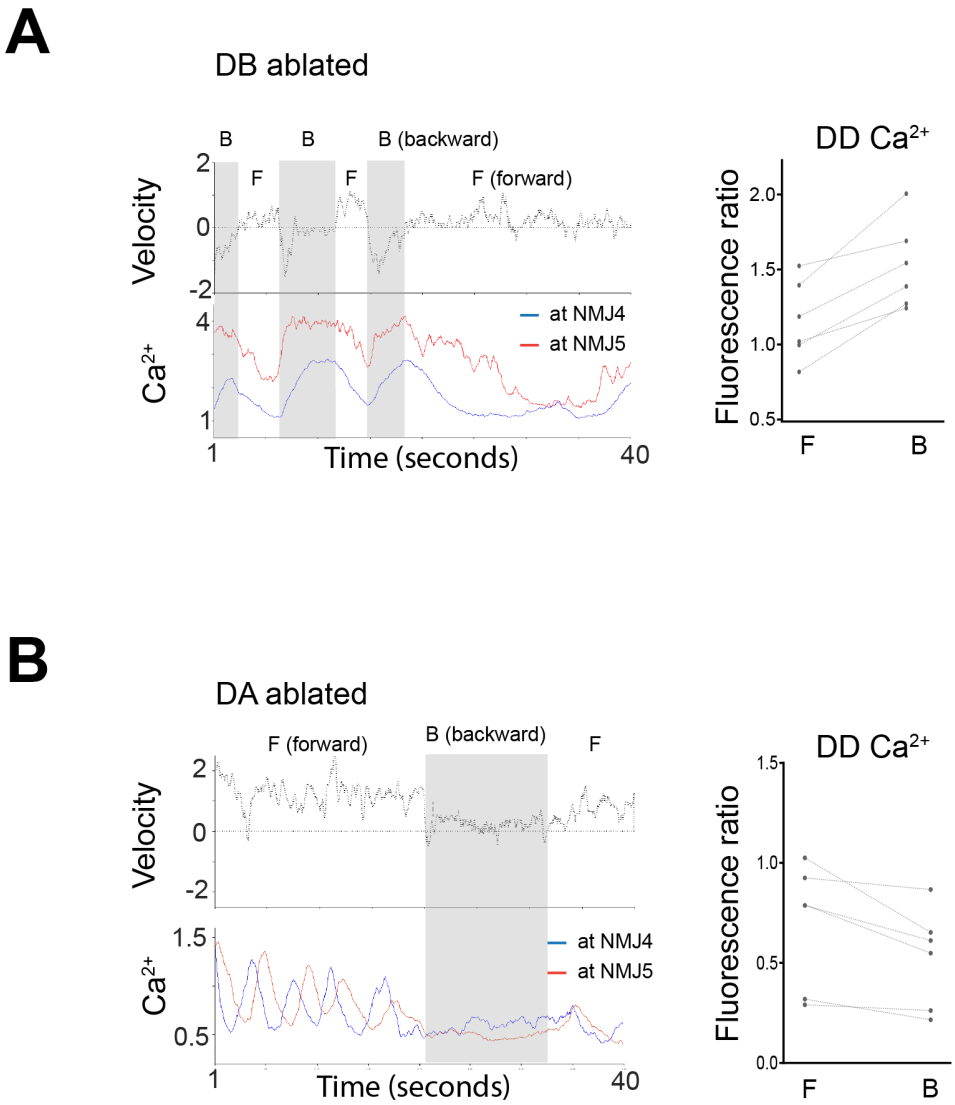

Figure S4. Ablation of cholinergic motor neurons reduces DD activity during directional movement. **A.** (Left) An example of the velocity and DD NMJ Ca2+ activity of an L1 lava upon DA motor neuron ablation. It still made switches between forward and backward movement, although the attempted backward movement was exhibited as halting. (Right), quantification of mean Ca activity during epochs of forward and backward movement of the same animal. **B.** (Left) An example of the velocity and DD NMJ Ca2+ activity of an L1 lava upon DB motor neuron ablation. It still made switches between forward and backward movement, although the attempted forward movement was exhibited as halting. (Right) Quantification of mean Ca activity during epochs of forward and backward movement of the same animal.

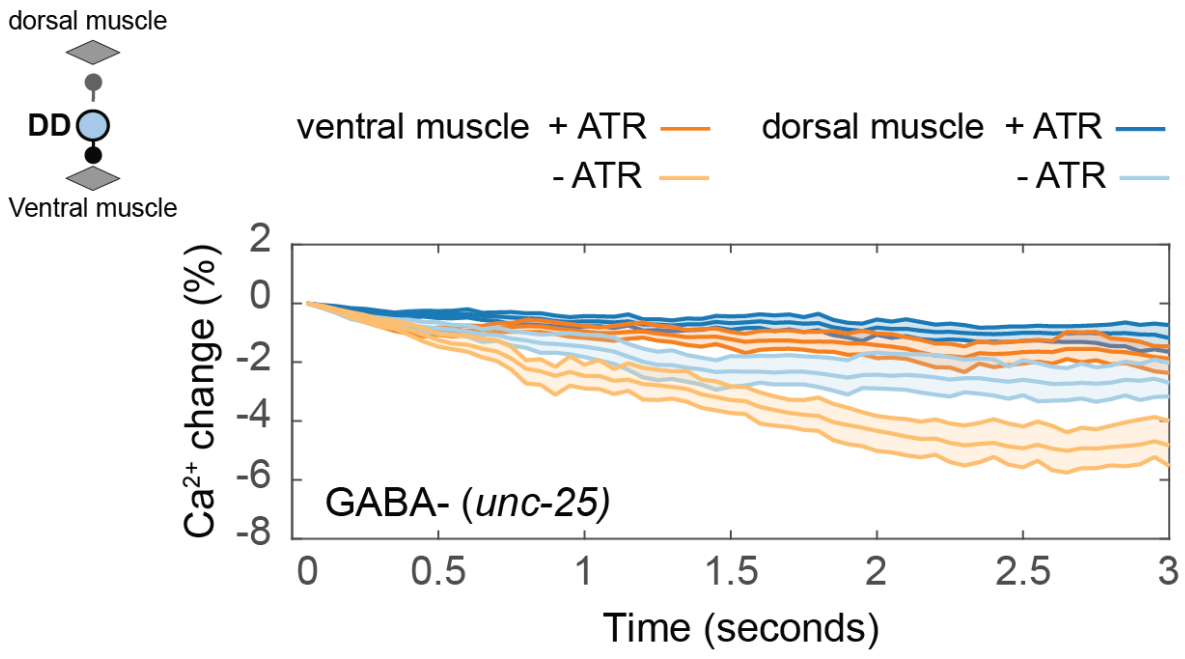

Figure S5. Activation of GABAergic motor neurons does not significantly reduce ventral and dorsal muscle activity in larva that do not synthesize GABA. Dorsal and ventral muscle calcium activity change upon optogenetic activation of DD motor neurons in L1 *unc-25* mutant larvae. Control group(-ATR): n = 34 stimulation events from 12 larvae; Experimental group(+ATR): n = 15 stimulation events from 5 larvae.

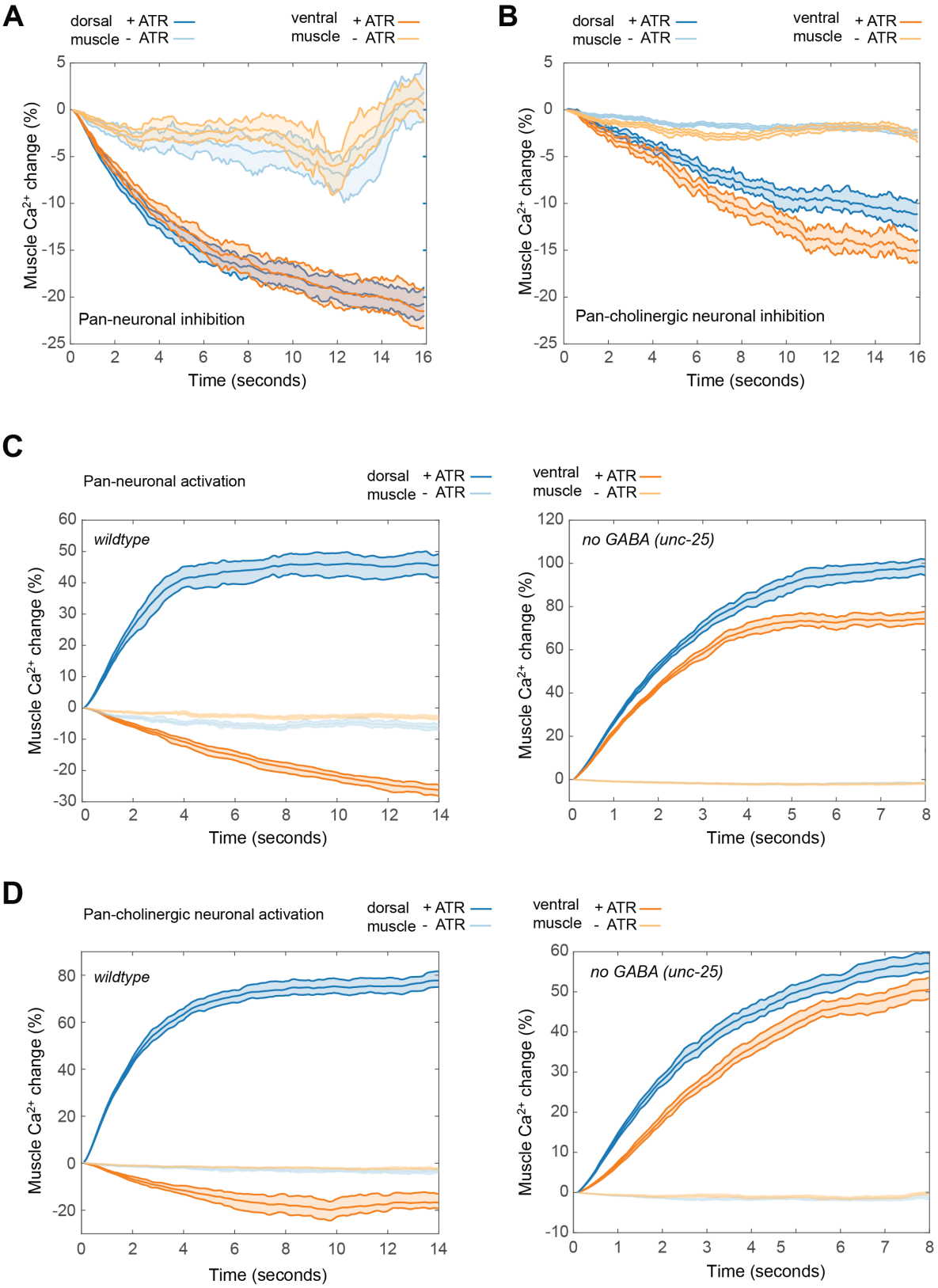

Figure S6. Effect of neuronal optogenetic manipulation on L1 larva's dorsal and ventral muscles A, B Muscle calcium responses upon optogenetic silencing panneuronally (A) or pan-cholinergic neuronally (B) in wildtype L1 larva. Panneuronal inhibition: -ATR: n = 18 stimulation from 6 larvae; +ATR:n = 26 stimulation from 12 larvae. Inhibition of cholinergic neurons: -ATR, n = 16 stimulation from 3 larvae; +ATR, n = 27 stimulation from 5 larvae.**C** Muscle calcium responses upon panneuronal optogenetic activation in wildtpye (left) or *unc-25* (right) L1 larvae. wildtype group: -ATR: n = 17 stimulation from 9 larvae; +ATR: n = 18 stimulation from 10 larvae. *unc-25* group: -ATR: n = 14 stimulation from 9 larvae; +ATR: n = 21 stimulation from 11 larvae. **D** Muscle calcium responses upon pan-cholinergic optogenetic activation in wildtpye (left) or *unc-25* (right) L1 larvae. wildtype group: -ATR, n = 15 stimulation from 7 larvae; +ATR, n = 19 stimulation from 10 larvae. *unc-25* group: -ATR, n = 18 stimulation from 6 larvae; +ATR, n = 30 stimulation from 10 larvae.

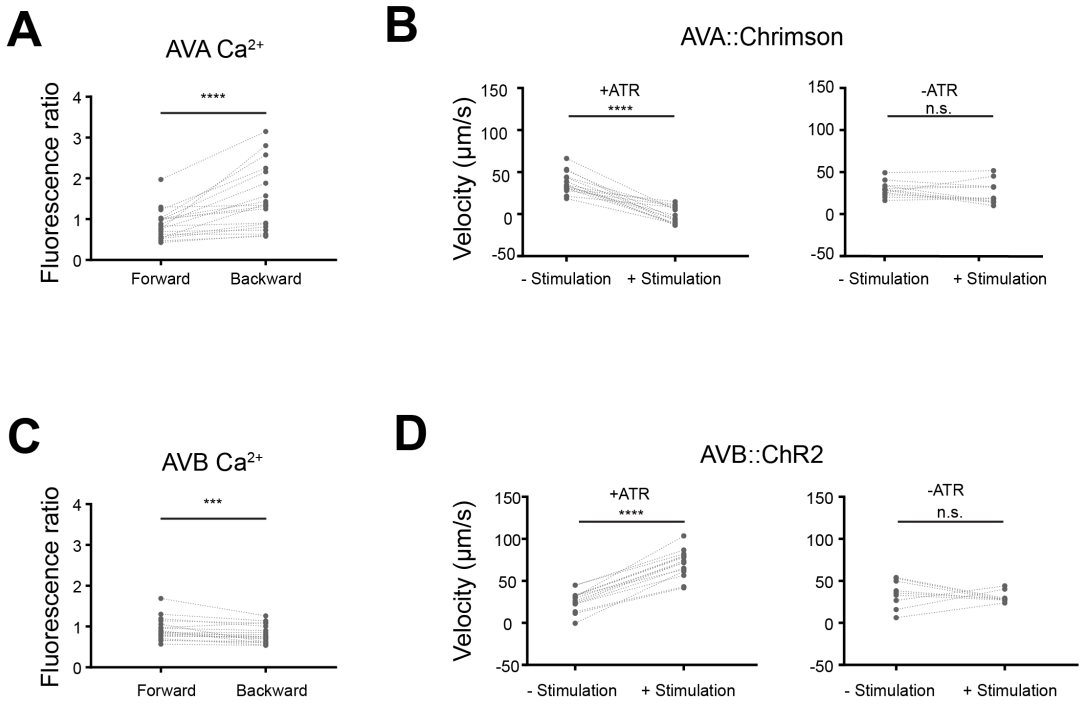

Figure S7. Subgroups of premotor interneurons potentiate directional movements in L1 larvae. **A.** The AVA premotor interneuron exhibits higher activity during backward than forward movements. n = 19 larvae **B.** Optogenetic activation of AVA leads to increased reversal velocity. Velocity during non-stimulated and stimulated phases was compared in the control (-ATR) group (n = 12 larvae, p = 0.2334) and the experimental (+ATR) group (n = 15 larvae, **** $p < 0.0001$). **C.** The AVB premotor interneurons exhibit higher activities during forward than during backward movements. n = 19, *** p = 0.0006. **D.** Optogenetic stimulation of AVB leads to increased forward velocity. For the control (- ATR) group, n = 9 larvae, p = 0.4961 between non-stimulated and stimulated period. For the experimental (+ ATR) group, n = 15 larvae, ****$p < 0.0001$. $p < 0.05$ was considered to be statistically significant. All analyses were performed by the Wilcoxon matched-pairs sign rank test.

Movie captions

Supplemental Movie 1 (Fig. 1C): L1 larva generates alternating dorsal and ventral body bends

a) An L1 larva swimming in the M9 solution. In the first frame, head is up and tail is down. A lump of bacteria food in the middle of the field anchors this happy baby. b) An L1 larva crawling on a NGM-culture plate coated with a thin layer of bacteria food. In the first frame, head is down, tail is up, dorsal is left, and ventral is right.

Supplemental Movie 2 (Fig. 1D): L1 larva generates off-phase, curvature-correlated dorsal and ventral muscle calcium dynamics

Calcium imaging of muscle cells of a crawling L1 larva. *Upper panels* Time-lapse imaging of a crawling L1 larva that expressed GCaMP3::RFP in all non-pharyngeal muscle cells. Head is left, tail is right, dorsal is up and ventral is down. GCaMP3/RFP ratio was segmented along the body. Color bar represents the same scale for the Y-axis of the lower panel. Dashed line denotes the segment that separates the head and the body. *Lower panel* Calcium signals in dorsal (blue) and ventral (red) muscles over time. X-axis represents body segments (head: 1; tail: 100); the vertical dashed line denotes the segment that separates the head and body. Y-axis represents GCaMP3/RFP value at each segment.

Supplemental Movie 3 (Fig. 2A): Sequential increase of DA motor neuron activity during L1 larva's backward movement.

Time-lapse calcium imaging of a crawling L1 larva expressing GCaMP6::RFP in the DA subclass of eMN motor neurons. Head: left; tail: right; dorsal: up; ventral: down. GCaMP6 and RFP signals from DA3-DA9 somata were tracked. Appearance of the left-pointing arrows denotes periods of forward movement; right-point arrows periods of backward movement. Grey bars denote periods of backward movement.

Supplemental Movie 4 (Fig. 2B): Sequential increase of DB motor neuron activity during L1 larva's forward movement.

Time-lapse calcium imaging of a crawling L1 larva expressing GCaMP6::RFP in all eMN motor neurons, but with a higher level in DBs. Head: left; tail: right; dorsal: up; ventral: down. GCaMP6 and RFP signals from DB4-6 somata were tracked. Appearance of the left-pointing arrows denotes periods of forward movement; right-point arrows periods of backward movement. Grey bars denote periods of forward movement.

Supplemental Movie 5 (Fig. 3A): NMJs from DD motor neurons are activated during both forward and backward movements.

Time-lapse calcium imaging of a crawling L1 larva expressing GCaMP6::RFP in DD neurons. Head: left; tail: right; dorsal: up; ventral: down. GCaMP6 and RFP signals from NMJs from DD5 and DA6 were tracked. Appearance of the left-pointing arrows denotes periods of forward movement; right-point arrows periods of backward movement. Grey bars denote periods of backward movement.

Supplemental Movie 6 (Fig. 3D, E): Activation of DD motor neurons elevates dorsal and ventral muscle activity, with different spatial patterns

Simultaneous iMN motor neuron optogenetic activation and muscle calcium imaging in an immobilized L1 larva. *Upper panels* Time-lapse imaging of a L1 larva that expressed GCaMP6::RFP in muscle cells and chrimson in DD motor neurons, and supplemented with ATR. Head is left, tail is right, dorsal is up and ventral is down. Dashed line denotes the body segment that separates the head and the body. *Lower panel* Calcium signals in dorsal (blue) and ventral (red) muscles over time. X-axis represents body segments (head: 1; tail: 100); the vertical dashed line denotes the segment that separates the head and body. Y-axis represents GCaMP6/RFP value at each segment.

Supplemental Movie 7 (Fig. 3F; Fig. 3S): Calcium signals in dorsal and ventral muscles exhibit distinct spatial patterns in a crawling L1 *unc-25* mutant larvae.

Calcium imaging of muscle cells of a crawling L1 larva that cannot synthesize GABA. *Upper panels* Time-lapse imaging of an *unc-25* mutant larva that expressed GCaMP3::RFP in all non-pharyngeal muscle cells. Head is left, tail is right, dorsal is up and ventral is down. GCaMP3/RFP ratio was segmented along the body. Color bar represents the same scale for the Y-axis of the lower panel. Dashed line denotes the body segment that separates the head and the body. *Lower panel* Calcium signals in dorsal (blue) and ventral (red) muscles over time. X-axis represents body segments (head: 1; tail: 100); the vertical dashed line denotes the segment that separates the head and body. Y-axis represents GCaMP3/RFP value at each segment.

Supplemental Movie 8a (Fig. 4): DD motor neurons are activated upon stimulation of DA and DB motor neurons.

Simultaneous eMN motor neuron optogenetic activation and iMN NMJ calcium imaging in an immobilized L1 larva. Time-lapse imaging of a L1 larva that expressed GCaMP6::RFP in DD motor neurons and chrimson in eMN motor neurons, and was supplemented with ATR. Head is left, tail is right, dorsal is up and ventral is down. NMJs from DD4 and DD5 were tracked. Right panel shows GCaMP6/RFP ratio normalized against the value at the first frame.

Supplemental Movie 8b (Fig.4): DD motor neurons are inactivated upon silencing of DA and DB motor neurons.

Simultaneous eMN motor neuron optogenetic activation and iMN NMJ calcium imaging in an immobilized L1 larva. Time-lapse imaging of a L1 larva that expressed GCaMP6::RFP in DD motor neurons and GtACR2 in eMN motor neurons, and was supplemented with ATR. Head is left, tail is right, dorsal is up and ventral is down. NMJs from DD5, DD6 and DD7 were tracked. Right panel shows GCaMP6/RFP ratio normalized against the value at the first frame.

Supplemental Movie 9 (Fig. 4A): Activation of eIN premotor interneurons induces spatially distinct calcium increase in L1 *unc-25* mutant larva's dorsal and ventral muscles

Simultaneous eIN premotor interneuron activation and muscle calcium imaging in an immobilized L1 larva that cannot

synthesize GABA. *Upper panels* Time-lapse imaging of an *unc-25* mutant larva that expressed GCaMP3::RFP in all non-pharyngeal muscle cells and ChR2 in AVA. Head is left, tail is right, dorsal is up and ventral is down. GCaMP3/RFP ratio was segmented along the body. Color bar represents the same scale for the Y-axis of the lower panel. Dashed line denotes the body segment that separates the head and the body. *Lower panel* Calcium signals in dorsal (blue) and ventral (red) muscles over time. X-axis represents body segments (head: 1; tail: 100); the vertical dashed line denotes the segment that separates the head and body. Y-axis represents GCaMP3/RFP value at each segment.

Supplemental Movie 10 (Fig. 6B): Silencing of eIN premotor interneurons reduces both dorsal and ventral muscle activities.
Simultaneous eIN premotor interneuron activation and muscle calcium imaging in an immobilized wildtype L1 larva. *Upper panels* Time-lapse imaging of a L1 larva that expressed GCaMP3::RFP in all non-pharyngeal muscle cells and chrimson in all eIN premotor interneurons. Head is left, tail is right, dorsal is up and ventral is down. GCaMP3/RFP ratio was segmented along the body. Color bar represents the same scale for the Y-axis of the lower panel. Dashed line denotes the body segment that separates the head and the body. *Lower panel* Calcium signals in dorsal (blue) and ventral (red) muscles over time. X-axis represents body segments (head: 1; tail: 100); the vertical dashed line denotes the segment that separates the head and body. Y-axis represents GCaMP3/RFP value at each segment.

Supplemental Movie 11 (Fig. 7A): Calcium signal in ventral muscles is reduced after ablation of eIN premotor interneurons in a wildtype L1 larva.
Calcium imaging of muscle cells of an un-constraint L1 larva on a NMG-culture plate, after eIN premotor interneuron ablation. *Upper panels* Time-lapse imaging of a larva that expressed GCaMP3::RFP in all non-pharyngeal muscle cells and miniSOG in all premotor interneurons. After photo-ablation, it adopted a body posture of dorsal coiling. GCaMP3/RFP ratio was segmented along the body. Color bar represents the same scale for the Y-axis of the lower panel. Dashed line denotes the body segment that separates the head and the body. *Lower panel* Calcium signals in dorsal (blue) and ventral (red) muscles over time. X-axis represents body segments (head: 1; tail: 100); the vertical dashed line denotes the segment that separates the head and body. Y-axis represents GCaMP3/RFP value at each segment.

Supplemental Movie 12 (Fig. 7B): Calcium signal in ventral muscles is reduced after ablation of eIN premotor interneurons in a *unc-25(e156)* mutant L1 larva.
Calcium imaging of muscle cells of an un-constraint mutant L1 larva that cannot synthesize GABA, after eIN premotor interneuron ablation. *Upper panels* Time-lapse imaging of a *unc-25* larva that expressed GCaMP3::RFP in all non-pharyngeal muscle cells and miniSOG in all premotor interneurons. After photo-ablation, it adopted a body posture of dorsal coiling. GCaMP3/RFP ratio was segmented along the body. Color bar represents the same scale for the Y-axis of the lower panel. Dashed line denotes the body segment that separates the head and the body. *Lower panel* Calcium signals in dorsal (blue) and ventral (red) muscles over time. X-axis represents body segments (head: 1; tail: 100); the vertical dashed line denotes the segment that separates the head and body. Y-axis represents GCaMP3/RFP value at each segment.

Supplemental Movie 13 (Fig. 7C): Calcium signals in ventral muscles is reduced when vesicle release is blocked in eIN premotor interneurons.
Muscle calcium imaging of an un-constraint L1 larva with vesicle release blocked in all eIN premotor interneurons. *Upper panels* Time-lapse imaging of a L1 larva that expressed GCaMP3::RFP in all non-pharyngeal muscle cells and TeTx in all premotor interneurons. It adopted a body posture of dorsal coiling. GCaMP3/RFP ratio was segmented along the body. Color bar represents the same scale for the Y-axis of the lower panel. Dashed line denotes the body segment that separates the head and the body. *Lower panel* Calcium signals in dorsal (blue) and ventral (red) muscles over time. X-axis represents body segments (head: 1; tail: 100); the vertical dashed line denotes the segment that separates the head and body. Y-axis represents GCaMP3/RFP value at each segment.

Supplemental Movie 14 (Fig. 7D): Blocking vesicle release of eMN motor neurons reveals uniformed calcium signals in ventral muscle of the L1 larva.
Muscle calcium imaging of an un-constraint L1 larva with vesicle release blocked in all eMN motor neurons. *Upper panels* Time-lapse imaging of a L1 larva that expressed GCaMP3::RFP in all non-pharyngeal muscle cells and TeTx in DA and DB motor neurons. GCaMP3/RFP ratio was segmented along the body. Color bar represents the same scale for the Y-axis of the lower panel. Dashed line denotes the body segment that separates the head and the body. *Lower panel* Calcium signals in dorsal (blue) and ventral (red) muscles over time. X-axis represents body segments (head: 1; tail: 100); the vertical dashed line denotes the segment that separates the head and body. Y-axis represents GCaMP3/RFP value at each segment.

Supplemental Movie 15 (Discussion): Complex bending defects of the L1 *unc-25* mutant larva
The *unc-25* L1 mutant larva could not synthesize GABA. They exhibit complex bending defects that are difficult to quality for ventral or dorsal bias. Qualitatively, they rest in a body posture with robust ventral bending across the body. When they are prompted to move, their forward movement do not exhibit overt dorsal or ventral bias, whereas their reversals include rapid ventral coils. Same trends are observed for both crawling and swimming.

Constructs and Strains

Transgenic ZM strains were generated by injecting plasmid or fosmid constructs (pJH) at 2-50ng/ul, with respective injection markers into indicated genetic backgrounds, to produce those with extra chromosomal arrays (hpEx). They were integrated into the genome by UV irradiation of the Ex lines followed by selective screening and outcrossing against N2 wild-type strains (hpIs). Other strains were acquired from either *CGC* or individual laboratories.

Table S1. Strains information

Strain	Genotype	Construct	Notes
N2	wild-type		
CB156	*unc-25(e156)* III		without GABA
CB407	*unc-49(e407)* III		without GABAa
ZM9062	*hpIs583* [Pacr-2s-miniSOG::UrSL2::wCherry + lin-15(+)]	pJH3626	iMN ablation
ZM9062	*hpIs583* [Pacr-2s-miniSOG::SL2::RFP+lin-15(+)]	pJH3626	eMN ablation
ZM11009	*hpEx4343*[Pacr-5-TeTx::RFP + Punc-4-TeTx::RFP + HygromycinR];	pJH2634; pJH2685	eMN chemical synapse blocked
ZM7971	*hpIs321*[Pnmr-1-miniSOG::UrSL2::wCherry + lin-15(+)]; hpIs331[Plgc55-miniSOG::UrSL2::wCherry + lin-15(+)]	pJH2827; pJH2890	eIN ablation
ZM11007	*hpEx4341*[Pnmr-1-TexTx::RFP + Plgc55s-TeTx::RFP + HygromycinR];	pJH4504; pJH2633	eIN chemical synapse blocked
ZM10206	*hpEx4080*[Prig-3-LoxP::BFP::LoxP::Chrimson::wCherry + Ptwk-40s-Cre + Pmyo-2-wCherry]	pJH4253; pJH4237	eIN (AVA) activation
ZM7419	*hpIs363*[Psra-11-ChR2::YFP + Pttx-3::RFP][61]		eIN (AVB+) activation
ZM8428	*hpIs459*[Punc-4-GCaMP6s::wCherry + lin-15(+)]	pJH3137	eMN (DA) Ca2+
ZM9128	*hpIs595*[Pacr-2s-GCaMP6s::wCherry + lin-15(+)]	pJH3666	eMN (DB) Ca2+
ZM7656	*hpIs365*[Punc-25-GCaMP3::wCherry + lin-15(+)]	pJH2999	iMN (DD) Ca2+
ZM10393	*hpIs592*[Pttr-39-Chrimson::wCherry + lin-15(+)]; hpIs595[Pacr-2s-GCaMP6s::wCherry + lin-15(+)]	pJH3557; pJH3666	eMN Ca2+ upon iMN activation
ZM10313	*hpIs593*[Pttr-39-Chrimson::wCherry + lin-15(+)]; hpIs459[Punc-4-GCaMP6s::wCherry + lin-15(+)]	pJH3718; pJH3717	eMN (A) Ca2+ upon iMN activation
ZM10823	*hpIs596*[Pacr-2s-Chrimson::wCherry + lin-15(+)]; hpIs268[Punc-25-GCaMP3::UrSL2::wCherry + lin-15(+)]	pJH3650; pJH2523	iMN Ca2+ upon eMN activation
ZM10440	*unc-49(e407)* III; hpIs592[Pttr-39-Chrimson::wCherry + lin-15(+)]; hpIs595[Pacr-2s-GCaMP6s::wCherry + lin-15(+)]	pJH3557; pJH3666	eMN Ca2+ upon iMN activation, without GABAa
ZM10673	*gbb-2(tm1165)* IV; hpIs592[Pttr-39-Chrimson::wCherry + lin-15(+)]; hpIs595[Pacr-2s-GCaMP6s::wCherry + lin-15(+)]	pJH3557; pJH3666	eMN Ca2+ upon iMN activation, without GABAb
ZM10585	*hpEx4177*[Pmyo-3::GtACR2::wCherry]; hpIs595[Pacr-2s-GCaMP6s::wCherry + lin-15(+)]	pJH4281; pJH3666	eMN Ca2+ upon muscle inactivation
ZM9585	*hpIs615*[Pacr-2s-Arch::wCherry + lin-15(+)]; hpIs365[Punc-25-GCaMP3::wCherry + lin-15(+)]	pJH3717; pJH2999	iMN Ca2+ upon eMN inactivation
ZM7691	*hpIs371*[Punc-4-miniSOG-SL2-wCherry + lin-15(+)]; hpIs365[Punc-25-GCaMP3::wCherry + lin-15(+)]	pJH2843; pJH2999	iMN Ca2+ upon eMN (A) ablation
ZM7798	*hpIs372*[Punc-5-miniSOG-SL2-wCherry + lin-15(+)]; hpIs365[Punc-25-GCaMP3::wCherry + lin-15(+)]	pJH2842; pJH2999	iMN Ca2+ upon eMN (B) ablation
ZM10281	*hpIs740*[Ptwk-40s-GCaMP6s::wScarlet]	pJH4260	eIN Ca2+
ZM10341	*hpIs717*[Pacr-2s-LoxP::BFP::loxP::Chrimson::wCherry + Punc-17-Cre + lin-15(+)]; hpIs740[Ptwk-40s-GCaMP6s::wScarlet + lin-15(+)]	pJH4140+pJH4143; pJH4260	eIN Ca2+ upon eMN activation
AQ2953	*ljIs131*[Pmyo-3::GCaMP3::SL2::tagRFP-T][62]		Muscle Ca2+
ZM10579	*hpEx4176*[Prgef-1-GtACR2::wCherry]; ljIs131[62]	pJH4329	Muscle Ca2+ upon panneural inactivation
ZM9648	*hpIs673*[Prgef-1-Chrimson::UrSL2::wCherry + lin-15(+)]; ljIs131[62]	pJH3628	Muscle Ca2+ upon panneural activation

ZM9660	*unc-25(e156)* III; hpIs673[Prgef-1-Chrimson::UrSL2::wCherry]; ljIs131[62]	pJH3628	Muscle Ca2+ upon panneural activation, without GABA
ZM10575	*hpEx4171*[Punc-17::GtACR2::wCherry]; ljIs131[62]	pJH4330	Muscle Ca2+ upon pan-cholinergic inactivation
ZM9429	*zxIs6*[Punc-17-ChR2::YFP]; ljIs131[62]		Muscle Ca2+ upon pan-cholinergic activation
ZM9573	*unc-25(e156); zxIs6*[Punc-17-ChR2::YFP]; ljIs131[62]		Muscle Ca2+ upon pan-cholinergic activation, without GABA
ZM10464	*hpEx4138*[Prgef-1-HisCl::UrSL2::wCherry]; ljIs131[Pmyo-3-GCaMP3::UrSL2::RFP]	pJH4407	Muscle Ca2+ upon panneural silencing
ZM10339	*hpIs717*[Pacr-2s-LoxP::BFP::LoxP::Chrimson::wCherry + Punc-17-Cre + lin-15(+)]; ljIs131[62]	pJH4140; pJH4143	Muscle Ca2+ upon eMN activation
ZM10340	*unc-25(e156)* III; *hpIs717*[Pacr-2s-LoxP::BFP::LoxP::Chrimson::wCherry + Punc-17-Cre + lin-15(+)]; ljIs131[62]	pJH4140; pJH4143	Muscle Ca2+ upon eMN activation, without GABA
ZM10458	*hpEx4134*[Pacr-2s-LoxP::BFP::LoxP::GtACR2::wCherry + Punc-17-Cre]; ljIs131[62]	pJH4211; pJH4143	Muscle Ca2+ upon eMN inactivation
ZM9131	*ljIs131*[Pmyo-3-GCaMP3::UrSL2::RFP]; *hpIs583* [Pacr-2s-miniSOG::SL2::RFP+lin-15(+)]	pJH3626	Muscle Ca2+ upon eMN ablation
ZM11020	*ljIs131*[Pmyo-3-GCaMP3::UrSL2::RFP]; *hpEx4343* [Pacr-5-TeTx::RFP + Punc-4-TeTx::RFP + HygromycinR]	pJH2634; pJH2685	Muscle Ca2+ upon eMN chemical synapse blocked
ZM9172	*unc-25(e156)* III; *ljIs131*[62]		Muscle Ca2+ without GABA
ZM10451	*unc-49(e407)* III; *ljIs131*[62]		Muscle Ca2+ without GABAa
ZM9313	*hpIs625*[Pttr-39-Arch::wCherry + lin-15(+)]; *ljIs131*[62]	pJH3718	Muscle Ca2+ upon iMN inactivation
ZM9551	*hpIs593*[Pttr-39-Chrimson::wCherry + lin-15(+)]; *ljIs131*[62]	pJH3557	Muscle Ca2+ upon iMN activation
ZM10176	*unc-25(e156)* III; *hpIs593*[Pttr-39-Chrimson::wCherry + lin-15(+)]; *ljIs131*[62]	pJH3557	Muscle Ca2+ upon iMN activation, without GABA
ZM10441	*unc-49(e407)* III; *hpIs592*[Pttr-39-Chrimson::wCherry + lin-15(+)]; *ljIs131*[62]	pJH3557	Muscle Ca2+ upon iMN activation, without GABAa
ZM10410	*gbb-2(tm1165)* IV; *hpIs593*[Pttr-39-Chrimson::wCherry + lin-15(+)]; *ljIs131*[Pmyo-3-GCaMP3::UrSL2::tagRFP]	pJH3557	Muscle Ca2+ upon iMN activation, without GABAb
ZM10411	*gbb-1(tm1406)* IV; *hpIs593*[Pttr-39-Chrimson::wCherry + lin-15(+)]; *ljIs131*[62]	pJH3557	Muscle Ca2+ upon iMN activation, without GABAb
ZM10743	*unc-49(e407)*; *gbb-2(tm1165)* IV; *hpIs592*[Pttr-39-Chrimson::wCherry + lin-15(+)]; ljIs131[Pmyo-3-GCaMP3::UrSL2::tagRFP]	pJH3557	Muscle Ca2+ upon iMN activation, without GABAa/b
ZM9119	*ljIs131*[Pmyo-3-GCaMP3::UrSL2::RFP]; hpIs559 [Pacr-5-miniSOG::SL2::BFP + Punc-4-miniSOG::SL2::BFP + Pttr-39-miniSOG::SL2::BFP + lin-15(+)]	pJH3439; pJH3449; pJH3458	Muscle Ca2+ upon all MN ablation
ZM7465	*hpIs321*[Pnmr-1-miniSOG::UrSL2::wCherry + lin-15(+)]; *hpIs331*[Plgc55-miniSOG::UrSL2::wCherry + lin-15(+)]; ljIs131[Pmyo-3-GCaMP3::UrSL2::RFP]	pJH2827; pJH2890	Muscle Ca2+ upon eIN ablation

ZM10484	*unc-25(e156)* III; *hpIs321*[Pnmr-1-miniSOG::UrSL2::wCherry + lin-15(+)]; *hpIs331*[Plgc55-miniSOG::UrSL2::wCherry + lin-15(+)]; *ljIs131*[Pmyo-3-GCaMP3::UrSL2::RFP]	pJH2827; pJH2890	muscle Ca2+ upon eIN ablation, without GABA
ZM10311	*unc-25(e156)*; *hpEx4080*[Prig-3-LoxP::BFP::LoxP::Chrimson::wCherry + Ptwk-40s-Cre + Pmyo-2-wCherry]; ljIs131[Pmyo-3::GCaMP3::UrSL2::tagRFP]	pJH4253;pJH4237	Muscle Ca2+ upon eIN (AVA) activation, without GABA
ZM10174	*unc-25(e156)*; *hpIs363*[Psra-11-ChR2::YFP+ Pttx-3::RFP][21]; *ljIs131*[Pmyo-3::GCaMP3::UrSL2::RFP]		Muscle Ca2+ upon eIN (AVB) activation, without GABA
ZM10552	*hpEx4081*[Prig-3-LoxP::BFP::LoxP::GtACR2::wCherry + Ptwk-40s-Cre + lin-15(+)]; *hpIs733*[Psra-11-LoxP::BFP::LoxP::GtACR2::wCherry + Ptwk-40s::Cre + lin-15(+)]; *ljIs131*[Pmyo-3::GCaMP3::UrSL2::tagRFP]	pJH4217; pJH4237; pJH4235; pJH4237	Muscle Ca2+ upon eIN inactivation
ZM11006	*ljIs131*[Pmyo-3-GCaMP3::UrSL2::RFP]; *hpEx4340* [Pnmr-1-TeTx::RFP + Plgc-55s-TeTx::RFP+HygromycinR]	pJH4505; pJH2633	Muscle Ca2+ upon eIN chemical synapse blocked
EN296	*unc-49(kr296::tagRFP)*		GABAa expression
ZM10926	*hpIs827* [GBB-1::GFP (fosmid) + Pmyo-2 RFP]	pJH4578	GABAb expression
ZM10829	*hpEx4271* [GBB-2::GFP (fosmid) + Pmyo-2 RFP]	pJH4579	GABAb expression